ANNUAL REVIEWS

Annual Review of Nuclear and Particle Science

A New Paradigm for Hadronic Parity Nonconservation and Its Experimental Implications

Susan Gardner,[1,4] W.C. Haxton,[2,4] and Barry R. Holstein[3,4]

[1]Department of Physics and Astronomy, University of Kentucky, Lexington, Kentucky 40506-0055

[2]Department of Physics, University of California, and Lawrence Berkeley National Laboratory, Berkeley, California 94720

[3]Department of Physics–LGRT, University of Massachusetts, Amherst, Massachusetts 01003

[4]Kavli Institute for Theoretical Physics, University of California, Santa Barbara, California 93016

Annu. Rev. Nucl. Part. Sci. 2017. 67:69–95

First published as a Review in Advance on August 7, 2017

The *Annual Review of Nuclear and Particle Science* is online at nucl.annualreviews.org

https://doi.org/10.1146/annurev-nucl-041917-033231

Copyright © 2017 by Annual Reviews. All rights reserved

ANNUAL REVIEWS **Further**

Click here to view this article's online features:

- Download figures as PPT slides
- Navigate linked references
- Download citations
- Explore related articles
- Search keywords

Keywords

hadronic parity violation, effective field theory, hadronic parity nonconservation

Abstract

The primary experimental goal of studies of hadronic parity nonconservation (PNC) has long been the isolation of the isovector weak nucleon–nucleon interaction, expected to be dominated by long-range pion exchange and enhanced by the neutral current. In meson-exchange descriptions, this interaction, together with an isoscalar interaction generated by ρ and ω exchange, dominates most observables. Both amplitudes have been used to compare and check the consistency of experiments, yet no evidence for isovector hadronic PNC has been found. We argue that the emphasis on isovector hadronic PNC was misplaced. The large-N_c expansion provides an alternative and theoretically better-motivated simplification of effective field theories (EFTs) of hadronic PNC, separating the five low-energy constants (LECs) into two of leading order (LO) and three of next-to-next-to-leading order (N^{2}LO). We show that this large-N_c LEC hierarchy accurately describes all existing data on hadronic PNC and discuss opportunities to further test the predicted large-N_c LEC hierarchy. This formalism—combined with future experiments—could lead to rapid progress in the next 5 years. We discuss the impact of anticipated new results and describe future experiments that can yield more precise values of the LO LECs and help to isolate the N^{2}LO $\sim$ 10% corrections.

Contents

1. INTRODUCTION

For more than two decades, the field of hadronic parity nonconservation (PNC) has struggled: The theoretical picture has been muddled, and very few new experiments have been done to help clarify matters. This situation is about to change. The creation of a high-intensity cold neutron beam line at the Spallation Neutron Source (SNS), as well as upgrades at the National Institute of Standards and Technology (NIST), will enable a new generation of experiments. Results from the first experiment performed at the SNS, the NPDGamma Collaboration's measurement of the γ-ray asymmetry $A_\gamma(\vec{n}p \rightarrow d\gamma)$, should be announced soon (1; see **http://meetings.aps.org/link/BAPS.2015.APR.S6.2**, **http://online.kitp.ucsb.edu/online/nuclear-c16/**). Furthermore, the feasibility of a new kind of "measurement"—the evaluation of PNC nucleon–nucleon (NN) scattering amplitudes from lattice QCD (LQCD)—has been demonstrated (2).

While such progress was being made, other developments have brought more clarity to the field, changing some of our prejudices and providing a new context for interpreting future results. First, it was discovered that the agreement between past experiments was better than had been recognized (3): Most of the tension that had existed was induced by flaws in global analyses of PNC. Second, a new proposal emerged for organizing the low-energy constants (LECs) that characterize hadronic PNC, based on large-N_c QCD (4, 5). We show here that this proposal accounts simply for all existing data—while illustrating that some of our past assumptions about hadronic PNC patterns were not justified. We describe these developments and discuss their implications for past and anticipated experiments, performing a new global experimental analysis that exploits the large-N_c LEC hierarchy.

NPDGamma is the latest effort to address one of the field's primary goals, measurement of PNC in the isovector NN interaction. In meson-exchange descriptions, this interaction is dominated by long-range pion exchange, with one πNN vertex governed by the weak interaction and the other by the strong. The weak πNN vertex h_π^1 has been of particular interest because of the expectation that it could help separate the roles of W and Z boson exchange in hadronic PNC, associated with

the four-currents J_W and J_Z that appear in the low-energy current–current Hamiltonian (6, 7)

$$\mathcal{H} = \frac{G_F}{\sqrt{2}}\left[J_W^\dagger J_W + J_Z^\dagger J_Z\right]. \qquad 1.$$

The charged current can be decomposed into two components, $J_W = \cos\theta_c J_W^0 + \sin\theta_c J_W^1$, where θ_c is the Cabibbo angle. The current J_W^0 drives the $u \to d$ transition and carries isospin and strangeness $\Delta I = 1$ and $\Delta S = 0$, whereas J_W^1 drives the $u \to s$ transition and carries $\Delta I = 1/2$ and $\Delta S = -1$. The neutral current also has two components, $J_Z = J_Z^0 + J_Z^1$; the first transforms as $\Delta I = 0$ and $\Delta S = 0$, and the second as $\Delta I = 1$ and $\Delta S = 0$. The current–current weak $\Delta S = 0$ *NN* interaction is then

$$\mathcal{H}^{\Delta S=0} = \frac{G_F}{\sqrt{2}}\left[\cos^2\theta_c J_W^{0\dagger} J_W^0 + \sin^2\theta_c J_W^{1\dagger} J_W^1 + J_Z^{0\dagger} J_Z^0 + J_Z^{1\dagger} J_Z^1 + J_Z^{0\dagger} J_Z^1 + J_Z^{1\dagger} J_Z^0\right]. \qquad 2.$$

The importance of isospin to this Lagrangian is clear: The symmetric product of two $\Delta I = 1$ J_W^0 currents transforms as $\Delta I = 0$ and 2, whereas the symmetric product of two $\Delta I = 1/2$ J_W^1 currents transforms as $\Delta I = 1$. Consequently, the charged-current contribution to the $\Delta I = 1$ weak *NN* interaction is suppressed by $\tan^2\theta_c \sim 0.04$, relative to the charged-current contributions to the $\Delta I = 0$ and 2 interactions. On the basis of this argument, it was concluded that the $\Delta I = 1$ component of the *NN* interaction would be dominated by the neutral current, which is of particular interest because it cannot be studied in strangeness-changing interactions due to the absence of tree-level flavor-changing neutral currents. The expectation of an important neutral-current contribution to the $\Delta I = 1$ PNC *NN* interaction has influenced PNC analyses since the 1980s.

The opportunity to take advantage of nuclei as laboratories to test an otherwise unconstrained Standard Model interaction has motivated both experiment and theory. By the mid 1980s, several advances had occurred:

1. Credible meson-exchange models of hadronic PNC had been developed that established "best values" and reasonable ranges for PNC weak couplings [e.g., the couplings of DDH (8)], including h_π^1.
2. A series of successful experiments measuring the circular polarization of the γ-ray from the decay of the 1.081-MeV $J^PI = 0^-0$ level in ^{18}F had been performed, testing the T = 1 mixing of this state with the nearby 0^+1 level at 1.042 MeV (9–13), but finding no signal at the $\sim 10^{-4}$ level.
3. A method to extract a limit on h_π^1 from these measurements was developed, exploiting a relationship between hadronic PNC and axial-charge β decay, largely eliminating any dependence on the choice of nuclear wave functions (14–16). Several high-quality measurements of the β decay rate were made (16).

This led to a surprising conclusion: The ^{18}F result, by itself or when combined with other measurements in a general hadronic PNC analysis (17), established an upper bound on h_π^1, relative to competing isoscalar amplitudes, that was approximately a factor of six below the DDH best value. The isoscalar amplitudes are somewhat stronger than expected, and the isovector considerably weaker. The analogy between this result and the $\Delta I = 1/2$ rule in strangeness-changing decays—where a similar anomaly in the ratio of $\Delta I = 3/2$ to $\Delta I = 1/2$ amplitudes is found—was immediately noted (17). These results show that the neutral current, once embedded in the strongly interacting environment of the nucleon, produces an effective coupling to the nucleon that is considerably weaker than had been expected from the elementary coupling to the quarks.

These results helped motivate the NPDGamma effort. The collaboration has worked toward its goal of measuring h_π^1 since approximately 2000, beginning with an earlier version of the experiment at LANSCE (18), then moving to the SNS to exploit the high-intensity cold neutron beam

line that became available there (1; see **http://meetings.aps.org/link/BAPS.2015.APR.S6.2**, **http://online.kitp.ucsb.edu/online/nuclear-c16/**). The goal has been to reach a sensitivity corresponding to $A_\gamma \sim 10^{-8}$ (19), verifying the ^{18}F result and possibly pushing beyond, to a detection of h_π^1. Experimental issues at LANSCE, including a weaker-than-anticipated neutron flux, led to a final result of $A_\gamma = [-1.2 \pm 2.1(\text{stat.}) \pm 0.2(\text{syst.})] \times 10^{-7}$ (18), comparable to the bound that had been set earlier by others (20). The effort to reach the 10^{-8} level was renewed on the high-intensity SNS beam line (see **http://meetings.aps.org/link/BAPS.2007.DNP.CD.5**). The DDH best-value prediction for A_γ is $\sim 5 \times 10^{-8}$.

The purpose of this review is to reexamine past experiments and consider anticipated new results, including those from NPDGamma, in the context of a new paradigm for hadronic PNC that arises when effective field theory (EFT) is combined with large-N_c requirements for treating the EFT's LECs. In the context of this scheme, not only ^{18}F but the entire set of hadronic PNC observations conform to a simple pattern. Our goal is to describe recent developments that have led to this satisfying conclusion. These include the following:

1. Modified constraints (3) extracted from the longitudinal asymmetry $A_L(\vec{p}p)$, at both low and intermediate energies, obtained when certain inconsistencies in past global hadronic PNC analyses were corrected.
2. An improved understanding of EFT approaches to hadronic PNC, ironing out some apparent differences between EFT descriptions (21–23) as well as establishing their effective equivalence to the traditional meson-exchange treatment, when the latter is restricted to low energies. The EFT approach leads to a description quite similar to Danilov's (24–26) early analysis in terms of S–P amplitudes, involving five degrees of freedom (or perhaps six if nuclear systems like ^{18}F are used, where the pion's range is important).
3. As we lack the data needed to perform a five- or six-dimensional analysis, the field has long employed simpler analyses with a smaller number of "most important" couplings. In the DDH meson-exchange model, h_π^1 and a corresponding vector-meson isoscalar coupling have been employed as the leading terms. However, as discussed below, this choice is both in conflict with experiment and lacking in theoretical justification. An alternative organizational scheme has recently been proposed, based on the large-N_c expansion, that appears to be compatible with all we have learned about hadronic PNC to date. This expansion identifies two alternative leading couplings, and predicts that subleading corrections to this scheme will enter at the relative order $1/N_c^2 \sim 10\%$. Here we assume that this suppression is effective despite the expected enhancement from long-range pion exchange.
4. This combined EFT/large-N_c approach leads to a leading-order (LO) two-dimensional (2D) characterization of hadronic PNC that uses the isotensor $^1S_0$–$^3P_0$ amplitude together with a specific combination of the isoscalar $^3S_1$–$^1P_1$ and $^1S_0$–$^3P_0$ amplitudes. We derive the LO LECs from current experiments, and show the general concordance between PNC observations and the coupling hierarchy predicted by the large-N_c scheme.
5. We describe further opportunities to test this picture, through new experiments and by using LQCD.
6. The ^{18}F and NPDGamma experiments probe observables that are blind to the LO couplings and arise only through N^{2}LO corrections. Thus, the absence of a ^{18}F signal is not in conflict with theory, but is in fact consistent with large-N_c predictions. We show that by combining the ^{18}F result with the anticipated NPDGamma measurement, important constraints can be placed on N^{2}LO couplings.

This article reviews the first three developments above, then addresses the last three points by performing a new global analysis using the EFT/large-N_c formalism.

2. BACKGROUND

The violation of parity invariance, suggested by Lee & Yang (27) in 1956, was discovered experimentally in 1957 by Wu et al. (28) via measurement of the $\boldsymbol{J}\cdot\boldsymbol{p}_e$ correlation parameter in the β decay of polarized ^{60}Co. It was immediately recognized that there should exist a corresponding PNC component of the *NN* interaction. The first experimental search for PNC was conducted in 1957 by Tanner (29), who sought evidence in the $^{19}\mathrm{F}(p,\alpha)^{16}\mathrm{O}$ reaction. Although the sensitivity of this measurement was not sufficient to observe a PNC signal, it was the first of a series of such experiments, which have continued to the present time, to detect subtle weak interaction effects in systems with strong and electromagnetic interactions. A summary can be found in various review articles (3, 17, 30, 31).

PNC has been observed in many hadronic systems, usually in the form of some pseudoscalar such as an asymmetry or a circular polarization, including cases where rather spectacular enhancements of the signal arise. Examples include the 2% photon circular polarization in the electromagnetic decay of an isomer of ^{180}Hf (32),

$$A_\gamma(^{180}\mathrm{Hf}^* \rightarrow {}^{180}\mathrm{Hf} + \vec{\gamma}) = -(1.66 \pm 0.18) \times 10^{-2}, \qquad 3.$$

and the nearly 10% longitudinal analyzing power for the scattering of polarized neutrons from ^{139}La (33),

$$A_b(\vec{n} + {}^{139}\mathrm{La}) = (9.55 \pm 0.35) \times 10^{-2}. \qquad 4.$$

These amplifications originate from chance nuclear-level near-degeneracies: States of the same spin but opposite parity can mix through the hadronic PNC interaction, generating a parity admixture inversely proportional to the energy splitting between the levels. Indeed, as the natural scale of hadronic PNC effects is $\sim G_\mathrm{F} m_\pi^2 \sim 10^{-7}$ (17), it is apparent that such enhancements can be many orders of magnitude.

With the development of theoretical frameworks for understanding hadronic PNC quantitatively, the field's attention switched from simply finding examples of PNC to identifying systems where PNC could be both measured and reliably interpreted in terms of the underlying PNC *NN* interaction. In an ideal world, such measurements would be carried out by studying the simple *NN* systems—*pp*, *np*, and *pn*—in the allowed threshold partial wave channels. As only one such measurement has been done at high precision, the field turned to few-nucleon systems, where techniques exist for solving the Schrödinger equation with realistic strong potentials. Certain selected light nuclei also provided reliable hadronic PNC constraints. Notable among these are ^{18}F and ^{19}F, where parity doublets enhance the experimental signal, and axial-charge β decay measurements can remove almost all of the usual nuclear structure uncertainties.

2.1. The Desplanques, Donoghue, and Holstein (DDH) Potential

Helping to drive these developments were theoretical descriptions of hadronic PNC defining what needed to be measured, and providing benchmark estimates of potential hadronic PNC signal sizes. The "standard" formalism for hadronic PNC experimental analysis became the meson-exchange model of DDH (8), which expresses the hadronic PNC potential in terms of the usual parity-conserving strong interaction meson–nucleon couplings defined by

$$\begin{aligned}\mathcal{H}_\mathrm{st} = {} & i g_{\pi NN} \bar{N} \gamma_5 \boldsymbol{\tau}\cdot\boldsymbol{\pi} N + g_\rho \bar{N}\left(\gamma_\mu + i\frac{\chi_\rho}{2m_N}\sigma_{\mu\nu}k^\nu\right)\boldsymbol{\tau}\cdot\boldsymbol{\rho}^\mu N \\ & + g_\omega \bar{N}\left(\gamma_\mu + i\frac{\chi_\omega}{2m_N}\sigma_{\mu\nu}k^\nu\right)\omega^\mu N, \qquad 5.\end{aligned}$$

where m_N is the nucleon mass. The numerical values assigned to the various couplings by DDH are $g^2_{\pi NN}/4\pi = 14.4$, $g^2_\rho/4\pi = (1/9)g^2_\omega/4\pi = 0.62$, $\chi_\rho = \kappa_p - \kappa_n = 3.70$, and $\chi_\omega = \kappa_p + \kappa_n = -0.12$. DDH employed the phenomenological PNC weak meson–nucleon Hamiltonian

$$\begin{aligned}\mathcal{H}_{\rm wk} = {} & i\frac{h^1_\pi}{\sqrt{2}}\bar{N}(\boldsymbol{\tau}\times\boldsymbol{\pi})_z N \\ & + \bar{N}\left(h^0_\rho \boldsymbol{\tau}\cdot\boldsymbol{\rho}^\mu + h^1_\rho \rho^\mu_z + \frac{h^2_\rho}{2\sqrt{6}}(3\tau_z\rho^\mu_z - \boldsymbol{\tau}\cdot\boldsymbol{\rho}^\mu)\right)\gamma_\mu\gamma_5 N \\ & + \bar{N}\left(h^0_\omega\omega^\mu + h^1_\omega\tau_z\omega^\mu\right)\gamma_\mu\gamma_5 N - h^{1'}_\rho\bar{N}(\boldsymbol{\tau}\times\boldsymbol{\rho}^\mu)_z\frac{\sigma_{\mu\nu}k^\nu}{2m_N}\gamma_5 N\,. \end{aligned} \qquad 6.$$

When Equations 5 and 6 are combined and a nonrelativistic reduction is made, a PNC potential is obtained with a specific spin and isospin structure, together with specific radial forms, governed by the meson masses. The coefficients of this potential are bilinears in the weak and strong couplings—these products are the parameters that can be extracted.

Provided that a consistent set of strong couplings is employed in global analyses, such a program would determine values for the weak couplings $h^1_\pi, h^{0,1,2}_\rho, h^{1'}_\rho$, and $h^{0,1}_\omega$. In their original work, DDH provided theoretical estimates for these parameters—while emphasizing their very large uncertainties. DDH provided a best guess for each parameter (which they referred to as the "best value"), as well as a "reasonable range" to provide a measure of the uncertainty (**Table 1**).

Despite a great deal of experimental and theoretical research, most of this uncertainty remains today. The main obstacle to reducing the reasonable ranges has been a lack of reliable experimental constraints. Critical examinations of the available data have led to the conclusion that only four observables place important constraints on hadronic PNC—the analyzing power for the scattering of longitudinally polarized protons off protons, the circular polarization of the γ-ray emitted from the 0^-0 excited state in ^{18}F, the analyzing power for the scattering of longitudinally polarized protons off ^{4}He, and the γ decay asymmetry from the decay of the polarized $\frac{1}{2}^-\frac{1}{2}$ state in ^{19}F. Both of the last two measurements involve odd-proton systems, and consequently yield almost the same constraint, whereas the ^{18}F result is only an upper bound (although a very significant one, given the DDH estimate of the best value for h^1_π).

To improve on the current situation, one needs either several new, interpretable experimental results or a strategy that reduces the number of theoretical variables that must be determined. Such a strategy has recently been proposed, based on large-N_c QCD. As this approach is most naturally described in terms of EFT treatments of hadronic PNC, we first describe that formalism and its relationship to the DDH potential.

Table 1 The weak meson–nucleon couplings[a,b]

Coupling	DDH (8) reasonable range	DDH (8) "best value"	DZ (34)	FCDH (35)
h^1_π	$0 \to 11$	$+4.6$	$+1.1$	$+2.7$
h^0_ρ	$11 \to -31$	-11	-8.4	-3.8
h^1_ρ	$-0.4 \to 0$	-0.2	$+0.4$	-0.4
h^2_ρ	$-7.6 \to -11$	-9.5	-6.8	-6.8
h^0_ω	$5.7 \to -10.3$	-1.9	-3.8	-5.0
h^1_ω	$-1.9 \to -0.8$	-1.2	-2.3	-2.3

[a] As estimated in References 8, 34, and 35.

[b] All numbers are quoted in units of 10^{-7}. Following the original treatment by DDH (8), $h^{1\prime}_\rho$ has been set to zero; it can be shown that at low energies this coupling is redundant (3).

2.2. The Effective Field Theory Picture

Although the DDH meson-exchange approach clearly contains some model dependence, it has stood as the standard language for analyzing low-energy PNC experiments for nearly four decades. In recent years, however, an alternative to the DDH potential has been developed, based on pionless EFT. Pionless EFT provides a model-independent formalism for describing experiments performed at momentum scales well below the pion mass, where the pion interaction becomes local. Most applications to PNC scattering satisfy this condition (36), at least with respect to the external momenta of the scattered particles. (If a nuclear bound state is involved, however, the nuclear Fermi momentum can also play a role.)

This approach was introduced in studies of hadronic PNC by Zhu et al. (21), although the roots of this kind of analysis reach back to Danilov's (24, 25) partial wave analysis and to the use of contact potentials by Desplanques & Missimer (37). The Zhu et al. formulation contained redundant terms that were later identified and eliminated by Girlanda (22). The EFT method was also developed by Phillips et al. (23). In pionless EFT, the *NN* interaction is represented by a small number of empirically determined contact terms. In the parity-conserving case, for example, there are only two, representing scattering lengths in the $^1S_0$ and $^3S_1$ channels. In the parity-violating case, however, there exist five low-energy S–P channels, and consequently five associated LECs.

Although the DDH and EFT approaches appear to be quite distinct, they are in fact operationally equivalent at the very low energies where pionless EFT is valid. This point was recently made by constructing an effective contact interaction that maps onto Danilov's partial wave analysis (3):

$$\begin{aligned} V_{\rm LO}^{\rm PNC}(\boldsymbol{r}) = {} & \Lambda_0^{^1S_0-{}^3P_0}\left(\frac{1}{i}\frac{\overleftrightarrow{\nabla}_A}{2m_N}\frac{\delta^3(\boldsymbol{r})}{m_\rho^2}\cdot(\boldsymbol{\sigma}_1-\boldsymbol{\sigma}_2)-\frac{1}{i}\frac{\overleftrightarrow{\nabla}_S}{2m_N}\frac{\delta^3(\boldsymbol{r})}{m_\rho^2}\cdot i(\boldsymbol{\sigma}_1\times\boldsymbol{\sigma}_2)\right) \\ & + \Lambda_0^{^3S_1-{}^1P_1}\left(\frac{1}{i}\frac{\overleftrightarrow{\nabla}_A}{2m_N}\frac{\delta^3(\boldsymbol{r})}{m_\rho^2}\cdot(\boldsymbol{\sigma}_1-\boldsymbol{\sigma}_2)+\frac{1}{i}\frac{\overleftrightarrow{\nabla}_S}{2m_N}\frac{\delta^3(\boldsymbol{r})}{m_\rho^2}\cdot i(\boldsymbol{\sigma}_1\times\boldsymbol{\sigma}_2)\right) \\ & + \Lambda_1^{^1S_0-{}^3P_0}\left(\frac{1}{i}\frac{\overleftrightarrow{\nabla}_A}{2m_N}\frac{\delta^3(\boldsymbol{r})}{m_\rho^2}\cdot(\boldsymbol{\sigma}_1-\boldsymbol{\sigma}_2)(\tau_{1z}+\tau_{2z})\right) \\ & + \Lambda_1^{^3S_1-{}^3P_1}\left(\frac{1}{i}\frac{\overleftrightarrow{\nabla}_A}{2m_N}\frac{\delta^3(\boldsymbol{r})}{m_\rho^2}\cdot(\boldsymbol{\sigma}_1+\boldsymbol{\sigma}_2)(\tau_{1z}-\tau_{2z})\right) \\ & + \Lambda_2^{^1S_0-{}^3P_0}\left(\frac{1}{i}\frac{\overleftrightarrow{\nabla}_A}{2m_N}\frac{\delta^3(\boldsymbol{r})}{m_\rho^2}\cdot(\boldsymbol{\sigma}_1-\boldsymbol{\sigma}_2)(\boldsymbol{\tau}_1\otimes\boldsymbol{\tau}_2)_{20}\right), \end{aligned} \qquad 7.$$

where $(\boldsymbol{\tau}_1\otimes\boldsymbol{\tau})_{20}\equiv(3\tau_{1z}\tau_{2z}-\boldsymbol{\tau}_1\cdot\boldsymbol{\tau}_2)/\sqrt{6}$. The subscripts on the LECs denote the change in isospin ΔI induced by the associated operator, and the superscripts indicate the specific PNC transition. With these operator definitions, the various Λs are dimensionless. Of course, there must exist a matching to the low-energy form of the DDH potential, yielding (3)

$$\begin{aligned} \Lambda_0^{^1S_0-{}^3P_0} &= -g_\rho(2+\chi_\rho)h_\rho^0-g_\omega(2+\chi_\omega)h_\omega^0 & {}^{\rm DDH}\Lambda_0^{^1S_0-{}^3P_0} &= 210, \\ \Lambda_0^{^3S_1-{}^1P_1} &= -3g_\rho\chi_\rho h_\rho^0+g_\omega\chi_\omega h_\omega^0 & {}^{\rm DDH}\Lambda_0^{^3S_1-{}^1P_1} &= 360, \\ \Lambda_1^{^1S_0-{}^3P_0} &= -g_\rho(2+\chi_\rho)h_\rho^1-g_\omega(2+\chi_\omega)h_\omega^1 & {}^{\rm DDH}\Lambda_1^{^1S_0-{}^3P_0} &= 21, \\ \Lambda_1^{^3S_1-{}^3P_1} &= \sqrt{\tfrac{1}{2}}\,g_{\pi NN}\left(\tfrac{m_\rho}{m_\pi}\right)^2 h_\pi^1+g_\rho(h_\rho^1-h_\rho^{1\prime})-g_\omega h_\omega^1 & {}^{\rm DDH}\Lambda_1^{^3S_1-{}^3P_1} &= 1340, \\ \Lambda_2^{^1S_0-{}^3P_0} &= -g_\rho(2+\chi_\rho)h_\rho^2 & {}^{\rm DDH}\Lambda_2^{^1S_0-{}^3P_0} &= 160, \end{aligned} \qquad 8.$$

where on the right the DDH-predicted "best values" have been employed, yielding values for the LECs (in units of 10^{-7}). Similarly, the EFT potentials of Girlanda (22) and Zhu et al. (21) must also be equivalent to Equation 7. The translation between the various formulations is given in the so-called Rosetta stone, table 2 of Reference 3.

This comparison shows that the DDH potential is effectively equivalent to pionless EFT at the low energies for which the latter is valid. In this regime, an S–P partial wave description is adequate, and five linear combinations of the seven DDH weak couplings describe the physics. The redundancy among these parameters is broken when P–D interactions become important. Then the meson masses also play an explicit role, as higher partial wave channels allow one to detect the noncontact form of the radial interaction. One can think of the DDH interaction as an EFT that is married to a physically motivated model, for the purpose of extending the interaction's range of validity to higher momenta.

However, regardless of what formulation one uses, there remains a major problem: Five parameters are needed to describe hadronic PNC in the low-momentum limit, but we do not have five reliable experimental constraints. Thus, some simplification is needed beyond that provided by EFT or by a low-momentum reduction of the DDH potential.

2.3. Experimental Constraints and Two-Dimensional Reductions

A standard display of experimental constraints on hadronic PNC was introduced in Reference 17 and has been in wide use ever since. It employs two parameters, not five, and was derived on largely empirical grounds—an after-the-fact examination of how theoretical predictions of PNC observables depend on the underlying weak couplings. In light of the discussion of the large-N_c expansion in Section 3, below, we sketch here how this standard display came about.

The current version of this plot is shown in **Figure 1**. It includes constraints from four types of experiments:

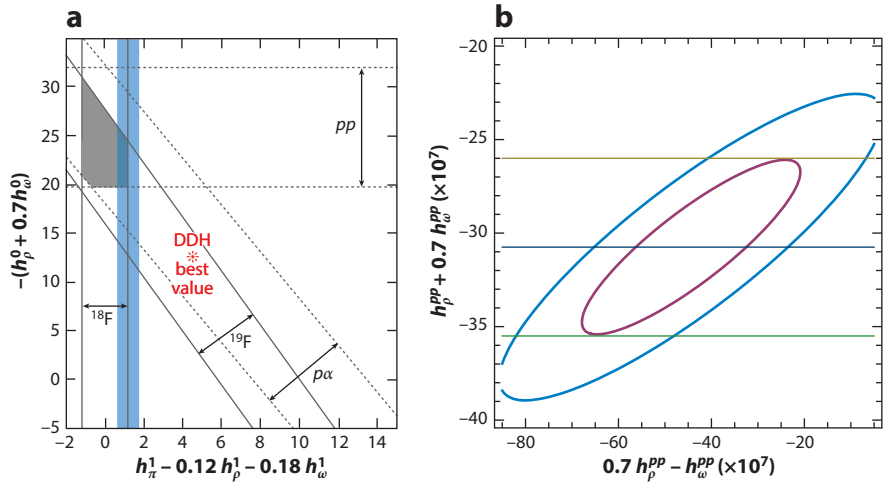

Figure 1

(*a*) The standard plot of experimental constraints on the DDH [Desplanques, Donoghue, and Holstein (8)] parameters, including recent revisions introduced in Reference 3. The experimental bands are 1σ. The vertical blue band comes from a preliminary estimate of h_π^1, based on a lattice QCD calculation of a three-point function (38). (*b*) Constraints on $h_{\rho,\omega}^{pp} = h_{\rho,\omega}^0 + h_{\rho,\omega}^1 + h_\rho^2/\sqrt{6}$ derived from $A_L(\vec{p}p)$ (3, 39). The ellipses represent the 68%- and 90%-CL contours.

1. The longitudinal analyzing power in the scattering of polarized protons from an unpolarized proton target, for which measurements were performed at 13.6 MeV at Bonn, 15 MeV at Los Alamos National Laboratory (LANL), 45 MeV at the Paul Scherrer Institut (PSI), and 221 MeV at TRIUMF:

$$A_{\rm L}(\vec{p}\,p) = \begin{cases} (-0.93 \pm 0.20 \pm 0.05) \times 10^{-7} & 13.6\,\text{MeV (40)} \\ (-1.7 \pm 0.8) \times 10^{-7} & 15\,\text{MeV (41)} \\ (-1.57 \pm 0.23) \times 10^{-7} & 45\,\text{MeV (42–44)} \\ (0.84 \pm 0.34) \times 10^{-7} & 221\,\text{MeV (45, 46)} \end{cases}. \quad 9.$$

The first three experiments were done at relatively low energy, where a description in terms of S–P amplitudes is a reasonable approximation. Thus, they constrain the partial wave coefficients of Equation 7 in a straightforward way (3, 39):

$$\Lambda_0^{^1\mathrm{S}_0-^3\mathrm{P}_0} + \Lambda_1^{^1\mathrm{S}_0-^3\mathrm{P}_0} + \frac{1}{\sqrt{6}}\Lambda_2^{^1\mathrm{S}_0-^3\mathrm{P}_0} = 419 \pm 43. \quad 10.$$

The *S–P* LECs Λ are given in units of 10^{-7}. The TRIUMF measurement, in contrast, must be treated in a formalism that includes higher partial waves in the weak interaction, such as the DDH potential. As shown in **Figure 1*a***, the resulting constraints on weak couplings can be expressed in terms of one combination related to S–P amplitudes, using the relations in Equation 8, and another associated with P–D amplitudes. We discuss this result in more detail in Section 3.2, below.

2. The longitudinal analyzing power for scattering 46-MeV polarized protons on a ^{4}He target was measured at PSI (47, 48) to be

$$A_{\rm L}(\vec{p}\alpha)\Big|_{46\,\text{MeV}} = -(3.3 \pm 0.9) \times 10^{-7}, \quad 11.$$

placing the following constraint on the S–P LECs (3, 47):

$$\Lambda_0^{^1\mathrm{S}_0-^3\mathrm{P}_0} + 0.89\Lambda_1^{^1\mathrm{S}_0-^3\mathrm{P}_0} + 0.75\Lambda_0^{^3\mathrm{S}_1-^1\mathrm{P}_1} + 0.32\Lambda_1^{^3\mathrm{S}_1-^3\mathrm{P}_1} = 930 \pm 253. \quad 12.$$

3. The circular polarization of photons emitted in the decay of the 1.081-MeV 0^-0 excited state of ^{18}F to the 1^+0 ground state is induced by PNC mixing of the 0^- state with the nearby 0^+1 state at 1.042 MeV (**Figure 2**). Consequently, this experiment selects out isovector hadronic PNC. Four independent experiments have yielded the limits

$$P_\gamma = \begin{cases} (-7 \pm 20) \times 10^{-4} & \text{Caltech/Seattle (9)} \\ (-10 \pm 18) \times 10^{-4} & \text{Mainz (11)} \\ (3 \pm 6) \times 10^{-4} & \text{Florence (12)} \\ (2 \pm 6) \times 10^{-4} & \text{Queens (13)} \end{cases}. \quad 13.$$

These results lead to the constraint (3, 14)

$$|\Lambda_1^{^3\mathrm{S}_1-^3\mathrm{P}_1} + 2.42\Lambda_1^{^1\mathrm{S}_0-^3\mathrm{P}_0}| < 340, \quad 14.$$

which implies a value of h_π^1 significantly below the DDH best value.

4. The γ decay angular asymmetry for the transition from the polarized 110-keV $\frac{1}{2}^-$ excited state in ^{19}F to the $\frac{1}{2}^+$ ground state has been measured, testing the parity mixing of these levels (**Figure 2**). The results,

$$A_\gamma = \begin{cases} (-8.5 \pm 2.6) \times 10^{-5} & \text{Seattle (16)} \\ (-6.8 \pm 1.8) \times 10^{-5} & \text{Mainz (49, 50)} \end{cases}, \quad 15.$$

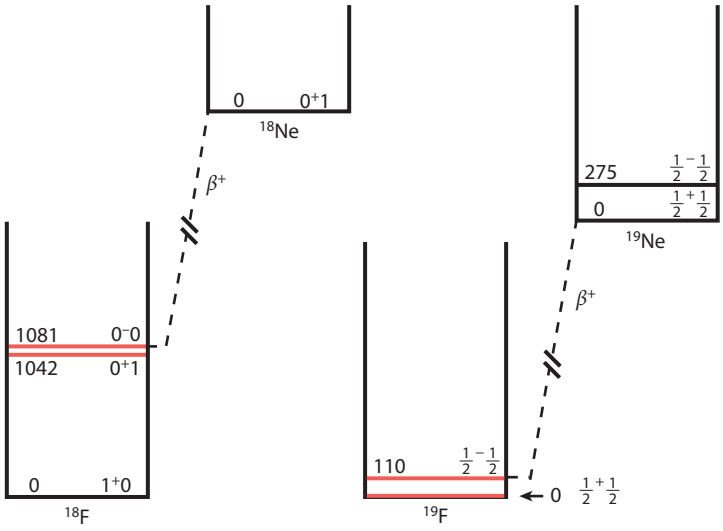

Figure 2

The parity doublets in ^{18}F and ^{19}F are indicated in red. The β^+ decays from ^{18}Ne and ^{19}Ne connect the negative-parity members of the parity doublets to the isotopic analogs of the positive-parity members (the ground states of ^{18}Ne and ^{19}Ne). These axial-charge β^+ decays can be used to calibrate the strength of the parity nonconservation doublet mixing. Energies are in keV.

constrain isoscalar and isovector hadronic PNC (3, 16):

$$\Lambda_0^{^1S_0-^3P_0} + 0.67\Lambda_1^{^1S_0-^3P_0} + 0.43\Lambda_0^{^3S_1-^1P_1} + 0.29\Lambda_1^{^3S_1-^3P_1} = 661 \pm 169. \qquad 16.$$

Note that this constraint is quite similar to that obtained from $\vec{p} + {}^4$He: Both systems involve an unpaired proton. As with ^{18}F, the nuclear mixing matrix element used in the analysis was determined from the axial-charge β decay of ^{19}Ne, linking the same states (up to an isospin rotation). The details of this determination can be found in Reference 16.

Figure 1 omits other constraints either because their interpretation is uncertain or because the measurements that have been done lack the precision needed to place meaningful constraints on hadronic PNC. Examples of the former include the anapole moment measurement for ^{133}Cs (51) and the circular polarization of the 2.789-MeV γ-ray emitted in the decay of ^{21}Ne (52, 53). The interpretations of these experiments depend on shell model estimates of quite complicated polarizabilities (Cs) or suppressed mixing matrix elements (^{21}Ne), and there are reasons to believe the associated errors could be large (3). The plot also omits hadronic PNC constraints established in experiments on neutron spin rotation in ^{4}He (54), on the longitudinal analyzing power for the capture of polarized protons on deuterium (41), on the circular polarization of γ-rays produced in the capture of unpolarized neutrons on hydrogen $np \to d\gamma$ (55), and on the γ-ray asymmetry from the capture of polarized neutrons on deuterium (56). The first three experiments established upper bounds that are not sufficiently restrictive to affect our analysis. The fourth experiment produced a signal much larger than expected, and for that reason is widely thought to reflect an unidentified experimental systematic.

Yet even with the restriction to four observables—$\vec{p}+p$, $\vec{p}+{}^4$He, $P_\gamma(^{18}\mathrm{F})$, and $A_\gamma(^{19}\mathrm{F})$—it is clear that all five partial wave amplitudes contribute to at least one of the observables. Early versions of **Figure 1** arose because it was noted that the observables plotted depended on very similar combinations of DDH isoscalar and isovector couplings—the combination $h_\rho^0 + 0.7h_\omega^0$ and

effectively h_π^1, with very small corrections due to h_ρ^1 and h_ω^1. Whereas isotensor PNC contributes to $A_L(\vec{p}\,p)$, it plays no role in the other observables. Because the purpose of the plot is to determine whether there is consistency among competing experiments, it thus made sense to "freeze out" this degree of freedom. This was done by "marginalizing" over the isotensor contribution, allowing it to vary over the DDH reasonable range, while fitting the isoscalar coupling to the measured $A_L(\vec{p}\,p)$. This procedure effectively expands the allowed pp band in **Figure 1**—although this expansion is modest because DDH assigned a relatively small reasonable-range uncertainty on h_ρ^2 of $\pm 20\%$.

We make several observations about **Figure 1**:

1. The figure shows a region of good overlap between the four experiments. For most of the past 15 years, similar plots showed some tension among the experiments, but recently it was found (3) that this tension originated largely from the use of inconsistent sets of strong interaction couplings in past analyses. As PNC experimental observables are bilinear in the weak and strong couplings, a fixed set of strong couplings must be used when extracting values of the DDH weak couplings. When the inconsistencies were corrected (3), the pp error band moved upward, increasing the region of overlap with the results from $\vec{p}+^4$He and ^{19}F. This is a welcome development, indicating that patterns are beginning to emerge from experiments.
2. Another motivation for **Figure 1** was to emphasize that certain combinations of weak couplings dominate most observables: Thus, in some LO sense, identifying patterns in hadronic PNC may not require a five-dimensional (5D) analysis. EFT approaches provide no guidance on such issues. In contrast, it is clear that certain DDH parameters (using their best values as a guide) are more important than others. Unfortunately, one of those parameters is h_π^1—undercutting any confidence one might have in relying on DDH for establishing the hierarchy of S–P couplings. This raises the question of whether some other theoretical basis exists for considering certain of the LECs as leading, and others as less important, allowing us to focus effort initially on establishing the values of the most important parameters.
3. **Figure 1** is 2D—but the end solution is consistent with $h_\pi^1 \sim 0$. Only one parameter is needed: the isoscalar strength. Had one known that at the start, one might have made another axis choice, using the isoscalar and isotensor directions to define a plane for displaying the experimental results.

Recently, a way to classify the S–P LECs as either leading or subleading has emerged from large-N_c analyses. That classification appears to be consistent with the hadronic PNC phenomenology described above, and provides a sound theoretical argument for focusing first on a particular 2D cut through the three-dimensional (3D) isoscalar–isotensor volume. In the context of large N_c, the absence of a signal from ^{18}F can be considered an important confirmation of an emerging pattern.

We now describe the new classification of LECs that emerges from large-N_c QCD, and we discuss how this classification influences our interpretation of existing and anticipated hadronic PNC data.

3. THE LARGE-N_c CLASSIFICATION AND EXPERIMENTAL IMPLICATIONS

The lovely large-N_c work of References 4 and 5 motivates us to pivot in the 5D space of LECs Λ to two new principal axes, one in the 2D $I = 0$ plane and one along the $I = 2$ direction,

$$\Lambda_0^+ \equiv \frac{3}{4}\Lambda_0^{^3S_1-{}^1P_1} + \frac{1}{4}\Lambda_0^{^1S_0-{}^3P_0} \sim N_c,$$
$$\Lambda_2^{^1S_0-{}^3P_0} \sim N_c, \qquad 17.$$

Table 2 A large-N_c hadronic PNC "Rosetta stone"[a,b]

Coefficient	DDH (8)	Girlanda (22)	Large N_c (5)
$\Lambda_0^+ \equiv \frac{3}{4}\Lambda_0^{^3S_1-{}^1P_1} + \frac{1}{4}\Lambda_0^{^1S_0-{}^3P_0}$	$-g_\rho h_\rho^0(\frac{1}{2}+\frac{5}{2}\chi_\rho) - g_\omega h_\omega^0(\frac{1}{2}-\frac{1}{2}\chi_\omega)$	$2\mathcal{G}_1 + \tilde{\mathcal{G}}_1$	$\sim N_c$
$\Lambda_0^- \equiv \frac{1}{4}\Lambda_0^{^3S_1-{}^1P_1} - \frac{3}{4}\Lambda_0^{^1S_0-{}^3P_0}$	$g_\omega h_\omega^0(\frac{3}{2}+\chi_\omega) + \frac{3}{2}g_\rho h_\rho^0$	$-\mathcal{G}_1 - 2\tilde{\mathcal{G}}_1$	$\sim 1/N_c$
$\Lambda_1^{^1S_0-{}^3P_0}$	$-g_\rho h_\rho^1(2+\chi_\rho) - g_\omega h_\omega^1(2+\chi_\omega)$	$\mathcal{G}_2$	$\sim \sin^2\theta_w$
$\Lambda_1^{^3S_1-{}^3P_1}$	$\frac{1}{\sqrt{2}}g_{\pi NN}h_\pi^1\left(\frac{m_\rho}{m_\pi}\right)^2 + g_\rho(h_\rho^1 - h_\rho^{1\prime}) - g_\omega h_\omega^1$	$2\mathcal{G}_6$	$\sim \sin^2\theta_w$
$\Lambda_2^{^1S_0-{}^3P_0}$	$-g_\rho h_\rho^2(2+\chi_\rho)$	$-2\sqrt{6}\mathcal{G}_5$	$\sim N_c$

[a]Low-energy constants for the S–P parity nonconservation (PNC) potential of Equation 7 are organized according to the large-N_c classification of Reference 5.

[b]The relationships to the DDH (8) potential and to the coefficients of Girlanda's (22) effective field theory potential are shown. Note that a multiplicative factor of $2m_N m_\rho^2$ must be applied to the Girlanda entries to obtain the dimensionless coefficients Λ, for instance, $\Lambda_1^{^1S_0-{}^3P_0} = \mathcal{G}_2\,[2m_N m_\rho^2]$.

with the remaining three orthogonal axes suppressed in the $1/N_c$ counting:

$$\begin{aligned} \Lambda_0^- \equiv \frac{1}{4}\Lambda_0^{^3S_1-{}^1P_1} - \frac{3}{4}\Lambda_0^{^1S_0-{}^3P_0} &\sim 1/N_c, \\ \Lambda_1^{^1S_0-{}^3P_0} &\sim \sin^2\theta_w, \\ \Lambda_1^{^3S_1-{}^3P_1} &\sim \sin^2\theta_w. \end{aligned} \qquad 18.$$

One can consider these three subdominant directions to be next-to-next-to-leading order (N^{2}LO), contributing only in relative order $\sim 1/N_c^2$: This is explicitly the case for the second isoscalar axis, whereas for the $\Delta I = 1$ amplitudes additional suppression is gained from the weak mixing angle, $\sin^2\theta_w/N_c \sim 1/12$. Consequently, the large-N_c classification may prove to be especially useful in hadronic PNC, with corrections only at the $\sim$10% level.

Table 2 is a large-N_c version of the Rosetta stone table in Reference 3. For the Girlanda coefficients, the key relationships are $\mathcal{G}_1 \sim \tilde{\mathcal{G}}_1 \sim N_c$ and $\mathcal{G}_1 + 2\tilde{\mathcal{G}}_1 \sim 1/N_c$ (5). The relationships to the DDH parameters are also shown. On computing DDH best-value equivalents and comparing them to large-N_c expectations, one finds

$$\begin{Bmatrix} {}^{\rm DDH}\Lambda_0^+ \\ {}^{\rm DDH}\Lambda_2^{^1S_0-{}^3P_0} \end{Bmatrix} = \begin{Bmatrix} 319 \\ 151 \end{Bmatrix} \qquad \begin{Bmatrix} {}^{\rm DDH}\Lambda_0^- \\ {}^{\rm DDH}\Lambda_1^{^1S_0-{}^3P_0} \\ {}^{\rm DDH}\Lambda_1^{^3S_1-{}^3P_1} \end{Bmatrix} = \begin{Bmatrix} -70 \\ 21 \\ 1340 \end{Bmatrix}, \qquad 19.$$

with the LO contributions on the left and the N^{2}LO contributions on the right. The units are 10^{-7}. There is a glaring discrepancy in the $\Lambda_1^{^3S_1-{}^3P_1}$ isovector channel, where the pion contributes. The DDH value for Λ_0^- is also not negligible.

3.1. Experimental Constraints on Large-N_c Low-Energy Constants

In addition to the above results, we expect to have a new constraint from NPDGamma in hand soon. NPDGamma data taking is finished, and the statistical uncertainty of the result has been given as approximately 13 ppb (see **http://meetings.aps.org/link/BAPS.2015.APR.S6.2**). Current efforts are focused on measuring and subtracting potential systematic effects, including an asymmetry associated with aluminum in the target window. Consequently, we express the

anticipated asymmetry as

$$|A_\gamma| < 1.3 \times 10^{-8}\epsilon \qquad 20.$$

under the conservative assumption that the result will be an upper bound (it need not be so), which we set at the statistical uncertainty, while including a parameter $\epsilon > 1$ that will account for consequences of systematic errors, including that associated with the aluminum subtraction. We then find (3, 57; see also References 58 and 59)

$$|\Lambda_1^{^3S_1-{}^3P_1}| < 270\epsilon. \qquad 21.$$

The numerical coefficient provides a measure of the potential impact of the result, given the anticipated statistical error. This bound is important because it is approximately as restrictive as that from $P_\gamma(^{18}\mathrm{F})$, but has a different dependence on the LECs.

We now express all five results discussed above in the large-N_c LEC basis, sequestering the N^{2}LO terms in brackets:

$$\begin{aligned}
\frac{2}{5}\Lambda_0^+ + \frac{1}{\sqrt{6}}\Lambda_2^{^1S_0-{}^3P_0} + \left[-\frac{6}{5}\Lambda_0^- + \Lambda_1^{^1S_0-{}^3P_0}\right] &= 419 \pm 43 && A_L(\vec{p}p),\\
1.3\Lambda_0^+ + \left[-0.9\Lambda_0^- + 0.89\Lambda_1^{^1S_0-{}^3P_0} + 0.32\Lambda_1^{^3S_1-{}^3P_1}\right] &= 930 \pm 253 && A_L(\vec{p}\alpha),\\
\left[|2.42\Lambda_1^{^1S_0-{}^3P_0} + \Lambda_1^{^3S_1-{}^3P_1}|\right] &< 340 && P_\gamma(^{18}\mathrm{F}),\\
0.92\Lambda_0^+ + \left[-1.03\Lambda_0^- + 0.67\Lambda_1^{^1S_0-{}^3P_0} + 0.29\Lambda_1^{^3S_1-{}^3P_1}\right] &= 661 \pm 169 && A_\gamma(^{19}\mathrm{F}),\\
\left[|\Lambda_1^{^3S_1-{}^3P_1}|\right] &< 270\epsilon && A_\gamma(\vec{n}p \to d\gamma). \qquad 22.
\end{aligned}$$

The LO approximation corresponds to ignoring the bracketed terms while solving the three remaining equations for Λ_0^+ and $\Lambda_2^{^1S_0-{}^3P_0}$. The best-value solution is $\Lambda_0^+ = 717$ and $\Lambda_2^{^1S_0-{}^3P_0} = 324$, with a nearly vanishing χ^2 [reflecting the almost exact overlap of the $A_L(\vec{p}\alpha)$ and $A_\gamma(^{19}\mathrm{F})$ bands]. The contour of $\chi^2 = 1$ (the fit has one degree of freedom) encloses the region shown in **Figure 3**.

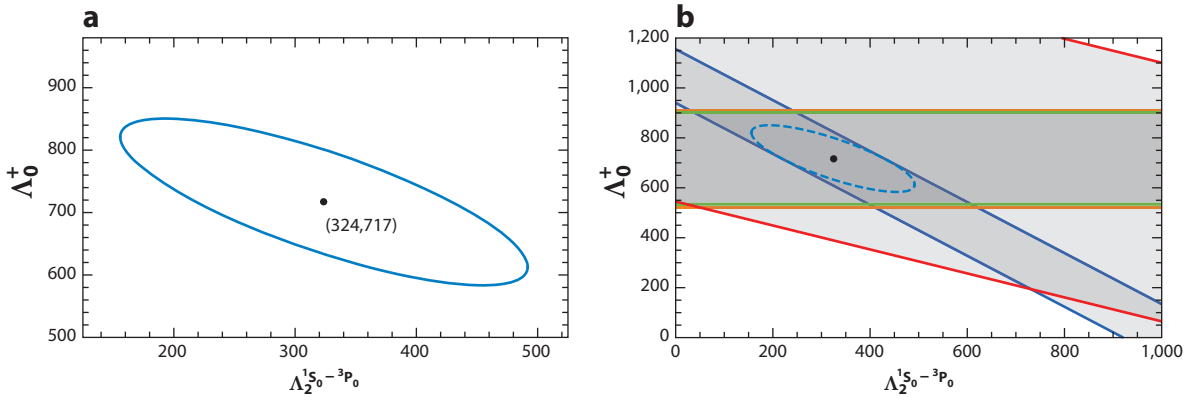

Figure 3

Leading-order large-N_c solutions satisfying all low-energy constraints on hadronic parity nonconservation. (*a*) An expanded view of the region, interior to the ellipse, with $\chi^2 < 1$. The dot marks the best-fit point. (*b*) The constraints from $A_L(\vec{p}p)$ at low energies (*blue boundary*), $A_L(\vec{p}\alpha)$ (*orange*), and $A_\gamma(^{19}\mathrm{F})$ (*green*), along with the combined allowed region (*dashed ellipse*), and $A_L(\vec{p}p)$ at 221 MeV (*red*). The experimental bands are 1σ. The low-energy constants are given in units of 10^{-7}.

Both of these best values are more than a factor of two larger than the DDH benchmark values for Λ_0^+ and $\Lambda_2^{^1S_0-{}^3P_0}$ given in Equation 19. This indicates that there may be a second shortcoming in **Figure 1**, from the perspective of large-N_c QCD: Not only were the wrong isospin axes used, but the marginalization that was done to remove the effects of $\Lambda_2^{^1S_0-{}^3P_0}$ from the band for $A_L(\vec{p}p)$ likely underestimated the associated uncertainties. In the procedures leading to **Figure 1**, it was assumed that the value for h_ρ^2, and consequently $\Lambda_2^{^1S_0-{}^3P_0}$, would be good to within the estimate reasonable range of ±20% around the best value. But the best-fit value we found is far outside this band. In fact, most of the allowed region for $\Lambda_2^{^1S_0-{}^3P_0}$ within the ellipse of **Figure 3** would also have been excluded by this band. Consequently, it is not surprising that there is a discrepancy between the isoscalar parameter employed in **Figure 1**, $-(h_\rho^0 + 0.7h_\omega^0)$, and that associated with Λ_0^+, $-(h_\rho^0 + 0.2h_\omega^0)$.

It is also apparent that there is no evidence for any nonzero contribution from the three N^{2}LO LECs. One way to illustrate this is to solve the three equalities above, turning on only one of the three N^{2}LO LECs while using the central experimental values. Doing so yields for the three choices, in turn,

$$(\Lambda_0^+, \Lambda_2^{^1S_0-{}^3P_0}, \Lambda_0^-) = (710, 309, -7),$$
$$(\Lambda_0^+, \Lambda_2^{^1S_0-{}^3P_0}, \Lambda_1^{^1S_0-{}^3P_0}) = (667, 199, 71),$$
$$(\Lambda_0^+, \Lambda_2^{^1S_0-{}^3P_0}, \Lambda_1^{^3S_1-{}^3P_1}) = (704, 336, 45).$$

In two cases, the resulting LO parameters do not move outside the $\chi^2 = 1$ ellipse of **Figure 3**, showing that any sensitivity to N^{2}LO parameters is buried under experimental noise. As the values of the N^{2}LO parameters are typically comparable to or less than the experimental uncertainties, we conclude that, with current data,

$$\Lambda_0^- \sim \Lambda_1^{^1S_0-{}^3P_0} \sim \Lambda_1^{^3S_1-{}^3P_1} \sim 0.$$

Thus, we do not have the number or quality of results needed to place meaningful constraints on parameters we expect to be approximately one-tenth the strength of the LO parameters. This helps to put the NPDGamma effort in context: It provides a key test of the efficacy of the large-N_c formalism through a first measurement of an N^{2}LO LEC.

3.2. The TRIUMF 221-MeV $A_L(\vec{p}p)$

As noted above, the DDH potential is equivalent to an EFT near threshold, and thus can be viewed as a model for extrapolating those results to higher momenta, where ranges controlled by meson masses become important and where additional degrees of freedom connected with P–D and other high partial wave amplitudes play a role. Conversely, we can work this process in reverse. The two axes of the ellipse in **Figure 1*b*** correspond to two constraints, one corresponding to the S–P component of the scattering and the second from the P–D component. The former we have already treated in the analysis of the low-energy data on $A_L(\vec{p}p)$, but the latter is additional. From equations 32 in Reference 3, we obtain the constraint

$$\Lambda_0^+ + 0.48\Lambda_2^{^1S_0-{}^3P_0} + \left[2.03\Lambda_0^- + 18.8(h_\rho^1 - h_\omega^1)\right] = 1{,}063 \pm 518 \qquad A_L(\vec{p}p)\Big|_{221\,\mathrm{MeV}}. \quad 23.$$

Note that a new isovector term arises, expressed in terms of DDH couplings, reflecting the fact that P–D scattering includes new degrees of freedom. For our just-determined best values for Λ_0^+ and $\Lambda_2^{^1S_0-{}^3P_0}$, the LO contribution to the left-hand side is 873. There is no evidence for any nonzero N^{2}LO contribution.

3.3. Deconstructing h_π^1: A "$\Delta I = 0$" Rule from Theory and Experiment

We have already noted that there is tension between the values we have found for Λ_0^+ and $\Lambda_2^{{}^1S_0-{}^3P_0}$ and the DDH best values; the large-N_c LO LECs are approximately a factor of two larger than their DDH predictions. Although uncertainties in our fit allow for values of $\Lambda_2^{{}^1S_0-{}^3P_0}$ as small as the DDH best value, such small values come at the cost of increasing Λ_0^+ even further (**Figure 3**). Thus, such an adjustment does not remove the tension.

An even larger discrepancy exists for $\Lambda_1^{{}^3S_1-{}^3P_1}$, as one can see by comparing the large-N_c predictions of Equations 17 and 18 with that of the DDH best values of Equation 19. The DDH best value is at least an order of magnitude larger than the naïve large-N_c expectation for an N^{2}LO parameter. This is the LEC to which one-pion exchange, and thus h_π^1, contributes. The purpose of this section is to describe the likely origin of this mismatch.

Equation 8 shows that the numerical value of ${}^{\rm DDH}\Lambda_1^{{}^3S_1-{}^3P_1}$ is dominated by the pion, as the contribution from vector-meson terms is less than 1% of the total. This dominance comes in part because the pion propagator at low momentum transfers generates a relative enhancement of $(m_\rho^2/m_\pi^2) \sim 30$, which magnifies the pion contribution to the ${}^{\rm DDH}\Lambda_1^{{}^3S_1-{}^3P_1}$ LEC and enhances this LEC relative to others. If we compare ${}^{\rm DDH}\Lambda^{{}^3S_1-{}^3P_1}$ with ${}^{\rm DDH}\Lambda_0^+$, we find no other large, distinguishing factors. For example, the DDH best-value effective pion coupling, $g_{\pi NN}h_\pi^1/\sqrt{32} \sim 1.08$, is comparable to those appearing in isoscalar channels, $-g_\rho h_\rho^0/2 \sim 1.59$ and $-g_\omega h_\omega^0/2 \sim 0.80$. Thus, one is led to conclude that a small value for ${}^{\rm DDH}\Lambda_1^{{}^3S_1-{}^3P_1}$, consistent with the large-N_c hierarchy, requires a significant reduction in the DDH best value for h_π^1—by a factor of 10 or more—to compensate for the propagator enhancement.

The anatomy of the h_π^1 coupling involves both the charged and neutral weak currents. An estimate for the charged current, or Cabibbo term, can be based on SU(3)$_f$ symmetry, either with (60–63) or without (64, 65) the use of PCAC and current algebra techniques. This contribution to the matrix element for $n \to p\pi^-$ can be related to known hyperon decays (61) as follows:

$$n_-^0 = -\left(\frac{2}{3}\right)^{1/2}\left[2\Lambda_-^0 - \Xi_-^-\right]\tan\theta_c \equiv g_\pi. \qquad 24.$$

Recalling that $\tan\theta_c = V_{us}/V_{ud}$ and using the Cabibbo–Kobayashi–Maskawa (CKM) fit of equation 12.27 in the CKM review of Reference 66, we find $\tan\theta_c = 0.231$. Using the experimental values in table 6.3 of Reference 67, but employing the phase conventions in appendix B of Reference 8, we find $g_\pi = 0.376 \times 10^{-7}$.

This charged-current contribution can be compared with the "best value" of h_π^1 from Reference 8, $h_\pi^1 \sim 12 g_\pi$, the value that was used in Equation 19. The difference reflects in part the neutral-current contribution, but also numerical factors associated with the renormalization group (RNG) evolution of the operators of the effective Hamiltonian to the low-momentum scale of interest. There are also SU(3)$_f$ breaking effects to consider. Before discussing these effects explicitly, we note that the methods that yield the so-called sum rule estimate of Equation 24 can also be used to compute n_0^0, the amplitude for $n \to n\pi^0$. In this case, were *CP* not broken, we should find $n_0^0 = 0$, as first noted by Barton (68). Indeed, this cancellation has been demonstrated explicitly (8), which serves as a consistency check of the method.

Turning to the balance of the terms in the $\Delta S = 0$ effective weak Hamiltonian, we find, unfortunately, that the methods used in the charged-current sector cannot be applied because they rely on the existence of $(V - A) \times (V - A)$ structures in the weak Hamiltonian. In this case, the needed πNN matrix elements have been estimated using a factorization ansatz when possible, supplemented by quark model estimates of the nonfactorizable contributions. These inputs, along with an estimate of the leading RNG evolution effects, yield the DDH best-value

estimate of $h_\pi^1 = (0.5 + 11.5)g_\pi = 12g_\pi$, where the separated factors indicate the charged- and neutral-current contributions, respectively (8).

However, this analysis has been revisited, particularly by Dubovik & Zenkin (DZ) (34), who extend the three-flavor analysis of DDH to include charm quarks and thus the possibility of GIM cancellation in loop effects (69). They also evaluate nonfactorizable contributions within the MIT bag model. Including operator mixing and RNG evolution, they find a smaller value of $h_\pi^1 \sim 4g_\pi$, but comparable values of h_ρ^1 and h_ω^1 (34). The possibility of Δ resonance contributions has been explored by Feldman et al. (35) in the DDH framework, and they have revisited h_π^1 as well, modifying the computation of the factorized contribution as well as that of the strong enhancement associated with the charged-current contribution to find $h_\pi^1 \sim 7g_\pi$. The updates made by Dubovik & Zenkin (34) and Feldman et al. (35) cannot be easily combined. We regard $h_\pi^1 \sim 1.3 \times 10^{-7}$ (34) as the better estimate.

The computations of h_π^1 we have considered thus far work within a constituent quark model framework, so that operators with strange quarks, albeit with no net strangeness, play no role. We consider model approaches that can address such operators as well. The possibility of a considerable enhancement within the context of factorization and dimensional analysis has been noted (70). This issue has been addressed in the Skyrme model. The two-flavor Skyrme model with vector mesons yields a small value of the order of $h_\pi^1 \sim 0.3 \times 10^{-7}$ (71), and thus comparable to g_π. A three-flavor Skyrme model, which can incorporate empirical baryon masses, magnetic moments, and hyperon decays fairly well, has been used to assess the role of four-fermion operators with $(\bar{q}q)(\bar{s}s)$ flavor structure, yielding values for h_π^1 in the range $(0.8 - 1.3) \times 10^{-7}$, considerably larger than the two-flavor result (72). The authors of Reference 72 stress that this result is not a consequence of a large (scalar) strangeness component in the nucleon wave function, a notion now in disfavor due to LQCD results (73–76), but rather of operators appearing that involve strange quarks. Note, however, that the effective PNC Hamiltonian they employ at a scale of $\sim$1 GeV includes neither QCD renormalization nor mixing effects in evolving from the weak scale. Such effects would presumably be muted, as noted by Dubovik & Zenkin (34), by the Glashow–Iliopoulos–Maiani (GIM) effects that can arise when the charm quark is included and could lead to additional cancellations. We note that a computation of the low-energy effective Hamiltonian including LO QCD evolution with heavy quarks has been made in the $\theta_c = 0$ limit (77); however, this is not a good approximation in the $\Delta I = 1$ sector, because the neutral-current contribution enters with a factor of $\sin^2\theta_w/3 \simeq 0.08$. For reference, the $|\Delta S| = 1$ low-energy effective Hamiltonian, with heavy quarks, has been computed to next-to-leading order (NLO) in QCD (78).

To conclude this section, we note that improved assessments of h_π^1 yield results that are considerably smaller than the "best estimate" given by DDH, and are less incompatible with the picture suggested by large N_c and naïve dimensional analysis. The emerging picture points to a dominance of the $\Delta I = 0$ hadronic PNC nucleon amplitudes relative to $\Delta I = 1$ ones, resulting from a combination of the suppression of the latter and a not-insignificant enhancement of the former, relative to DDH best values. This is reminiscent of the dominance of the $\Delta I = 1/2$ amplitude in $K \to \pi\pi$ decay, as was originally pointed out in Reference 17 (see also the recent work in References 79 and 80).

4. NEXT STEPS

The above arguments show that five significant experimental constraints on hadronic PNC—$A_L(\vec{p}p)$ near threshold and at 221 MeV, $A_L(\vec{p}\alpha)$, $P_\gamma(^1\mathrm{F})$, and $A_\gamma(^{19}\mathrm{F})$—are in excellent agreement

with expectations arising from large-N_c QCD. In particular, this approach provides two LO parameters, Λ_0^+ and $\Lambda_2^{^1S_0-{}^3P_0}$, that can be determined from the existing experiments, and appear to account very well for all observations. Three S–P N^{2}LO LECs, expected to be ∼10% of the LO LECs, do appear to be smaller; at least, no existing experiment requires assigning a nonzero value to any of the nonleading LECs. Large N_c thus provides a hierarchical simplification of standard EFT approaches, breaking the five degrees of freedom into a two-plus-three pattern. As discussed above, such a simplification has previously been attempted, but without sound motivation, leading to descriptions that in hindsight appear flawed. In contrast, the large-N_c hierarchy appears to be sound from the vantage points of both theory and experiment, and particularly useful for hadronic PNC because the correction terms are N^{2}LO, not NLO. This approach provides us with a sensible starting point for planning future research to refine our characterization of the hadronic weak interaction, and thus to understand how this interaction is modified when embedded in strongly interacting systems.

4.1. Testing the Leading-Order Theory

Despite the quality of the LO fit, there is not a great deal of redundancy, especially with the constraints from $A_L(\vec{p}\alpha)$ and $A_\gamma(^{19}F)$ being so similar. Thus, an additional independent measurement that is sensitive to the LO couplings would be valuable. Furthermore, whereas the value of $A_L(\vec{p}p)$ is known to 10%, the errors on the other two experiments exceed 25%. A new measurement matching the precision of $A_L(\vec{p}\,p)$, but probing a different combination of Λ_0^+ and $\Lambda_2^{^1S_0-{}^3P_0}$, could substantially shrink the allowed ellipse shown in **Figure 3**. A more precise determination of the LO LECs would be important for future searches for N^{2}LO LECs: In experiments where these terms arise in combination with LO terms, even modest errors in LO parameters would obscure the effects of N^{2}LO corrections. There do appear to be opportunities to generate new, high-quality constraints on the LO parameters.

4.1.1. Lattice QCD. In LQCD one solves strongly interacting problems by replacing the continuum problem with a discretized version, a finite grid in Euclidean space-time with periodic boundary conditions. Although doing so precludes any direct calculation of scattering amplitudes (81), the distortion of the energy levels in a finite volume can be related to low-energy scattering parameters (82–84) using techniques developed by Lüscher (85, 86). Most *NN* scattering calculations documented in the literature were performed with nuclear sources that placed both nucleons at the same space-time point, limiting the results to s-waves. In contrast, applications to hadronic PNC, where p-waves are clearly essential, require the use of extended nuclear sources, placed on the lattice in a variety of configurations that, in sum, allow one to associate lattice eigenvalues with partial waves having good spherical symmetry. This is a nontrivial problem, given the cubic symmetry of the lattice. The first calculation of parity-odd two-nucleon scattering using Lüscher's method was recently performed, demonstrating the technique (87).

Efforts are under way to apply LQCD to the problem of calculating $\Lambda_2^{^1S_0-{}^3P_0}$ (2). Because this scattering amplitude carries $\Delta I = 2$, there are no disconnected (quark-loop) contributions (88). Thus, the statistical noise in this channel should be significantly lower than in $\Delta I = 0$ and 1 channels, opening up the possibility of a good LQCD "measurement" near the physical pion mass. A calculation of hadronic PNC in the $\Delta I = 2$ channel is expected to be an order of magnitude less costly than a measurement in the $\Delta I = 1$ channel. Preliminary research on $\Delta I = 2$ *NN* PNC yielded a nonzero signal (2), and led to the identification of improved interpolating operators, significantly reducing the contamination from nucleon excited states at early times, at least for the

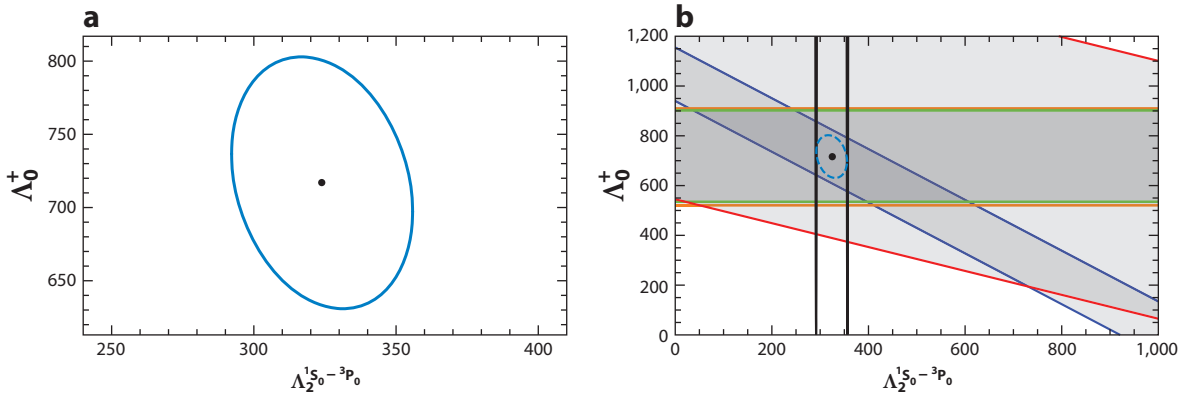

Figure 4

A modified version of **Figure 3** showing the constraint provided by the addition of a future lattice QCD calculation of the $\Delta I = 2$ amplitude $\Lambda_2^{^1S_0-{}^3P_0}$ to ±10%, centered on the central value from **Figure 3**. (*a*) An expanded view of the region, interior to the ellipse, with $\chi^2 < 1$. The dot marks the best-fit point. (*b*) The constraints from $A_L(\vec{p}p)$ at low energies (*blue boundary*), $A_L(\vec{p}\alpha)$ (*orange*), and $A_\gamma(^{19}\mathrm{F})$ (*green*), and the combined allowed region (*dashed ellipse*), in addition to leading-order large-N_c solutions satisfying all low-energy constraints on hadronic parity nonconservation. The experimental bands are 1σ. The low-energy constants are given in units of 10^{-7}.

heavy-pion masses ($m_\pi \sim 700$ and ∼800 MeV) that were used in these exploratory calculations. Phenomenologically relevant calculations will likely require calculations with $m_\pi \lesssim 300$ MeV, where valid comparisons can be made to low-energy EFTs (89–94).

The gestation period for major experiments in hadronic PNC, such as NPDGamma, can approach a decade or more. Recent improvements in LQCD applications to *NN* interactions have been rapid, and the basic tools are in place for a major attack on $\Lambda_2^{^1S_0-{}^3P_0}$. Thus, LQCD might turn out to be the fastest route to determining $\Lambda_2^{^1S_0-{}^3P_0}$ to the desired precision of 10%. The impact of such a result (**Figure 4**) would be quite significant.

Wasem (38) performed an early, exploratory calculation of h_π^1 in LQCD at $m_\pi \sim 389$ MeV. Instead of an *NN* amplitude, a three-point function (95) corresponding to a nucleon-to-resonance transition through pion absorption was calculated. The calculation did not include nonperturbative renormalization of the bare PNC operators, a chiral extrapolation to the physical pion mass, or the contributions from disconnected (quark-loop) diagrams. The result obtained, $h_\pi^1 = (1.10 \pm 0.51 \pm 0.06) \times 10^{-7}$, is consistent with the ^{18}F upper bound $|h_\pi^1| \lesssim 1.3 \times 10^{-7}$. The recent developments we have described for direct calculations of *NN* PNC amplitudes now supersede this approach.

4.1.2. New experiments constraining leading-order low-energy constants. Although one could envision developing new experiments to complement existing measurements on $A_L(\vec{p}p)$, it strikes us that the most conservative strategy might be to reexamine previous efforts on $A_L(\vec{p}\alpha)$ and $A_\gamma(^{19}\mathrm{F})$ to determine whether improvements are possible. Specifically, our analysis uses results from Lang et al.'s (47) 1985 measurement of $A_L(\vec{p}\alpha) = (-3.34 \pm 0.9) \times 10^{-7}$, which was performed with a 1.3-μA polarized beam from the Swiss Institute for Nuclear Research cyclotron. The beam's polarization was switched at the ion source every 30 ms. The experiment utilized techniques that the group had developed in its earlier $A_L(\vec{p}p)$ experiment (42–44) to control systematics. If the 1σ error bar on this result could be reduced by a factor of ∼2.5, the desired precision of ∼10% would be reached.

From the error budget provided, and under the assumption that the statistical and systematic errors were added in quadrature in forming the final result, it appears that the statistical contribution is somewhat larger. Thus, an experiment delivering about an order of magnitude more beam on target, combined with a reduction in the systematic error of approximately a factor of two, could be required. The latter will be challenging: The PSI group worked very hard to measure and correct for residual transverse components in the polarized beam, induced by nonuniform magnetic fields in the cyclotron. This was the principal systematic. Thus, a new experiment would need to do even better. Nevertheless, it strikes us that such an approach that builds on past experience, with a proven technology, and with sources of systematic error well documented could be preferable to starting an effort that lacks such a history.

The few-body theory used to relate the measurements to *NN* S–P amplitudes should also be updated. Several modern techniques could be applied to this problem, including quantum Monte Carlo (96).

Alternatively, one could consider a new attempt on $A_\gamma(^{19}\mathrm{F})$, one of two cases in which axial-charge β decay is available as a nuclear matrix element calibration. An important aspect of this experiment is the success in controlling systematic errors: An analysis (49) found that systematic errors were negligible, contributing to the overall uncertainty at a level that would have allowed a 10% measurement had the statistics been available. Thus, a repetition of this experiment with a factor-of-20 increase in counting could reach the target 10% uncertainty. As ^{19}F was produced using a relatively modest 0.4-μA 5-MeV polarized proton beam, the needed statistics might be attainable.

4.2. Testing the Next-to-Next-to-Leading-Order Theory: NPDGamma and $P_\gamma(^{18}\mathrm{F})$

A significant outcome of our research is the recognition that (*a*) past experiments have done a good job of characterizing the LO large-N_c interaction—with further improvements possible in the near term, such as that illustrated in **Figure 4**—and (*b*) we have already embarked on a credible campaign to learn about the N^{2}LO corrections. Concerning this second point, the striking aspect of Equation 22 is that $\Lambda_1^{^1\mathrm{S}_0-^3\mathrm{P}_0}$ and $\Lambda_1^{^3\mathrm{S}_1-^3\mathrm{P}_1}$ are the low-hanging fruit in this endeavor, because we can use isospin to restrict ourselves to the $\Delta I = 1$ plane in our 5D parameter space, where no LO terms exist to mask the smaller effects we seek. Furthermore, we have already embarked on a nearly optimal program to limit or measure these parameters: $P_\gamma(^{18}\mathrm{F})$ and NPDGamma are ideal choices for this task.

An important question to ask is where we might stand once NPDGamma announces its result. To assess this question we make the choice $\epsilon \sim 1$, which is a possible outcome because the important systematic effects in the experiment appear to be isolated in the window subtraction, including Al as the dominant correction. **Figure 5** shows the net results that would follow from combining the bound on $P_\gamma(^{18}\mathrm{F})$ with an NPDGamma $A_\gamma(\vec{n}p \to d\gamma)$ result centered on zero with a final error bar of 1.3×10^{-8}. Note that a central value for A_γ other than zero would shift the horizontal band up or down, whereas significant residual systematic uncertainties leading to $\epsilon > 1$ would broaden the band proportionately. One observes that the two experiments are very complementary, probing different combinations of the two $\Delta I = 1$ LECs. If one uses $\Lambda_0^+ \sim 700$ as the scale of the LO contribution, then current $P_\gamma(^{18})$F and potential NPDGamma constraints are approximately a factor of three below the LO scale, or roughly at the NLO level. Thus, considerable work remains to be done, as these constraints should be improved by another factor of three if the LECs are of natural size.

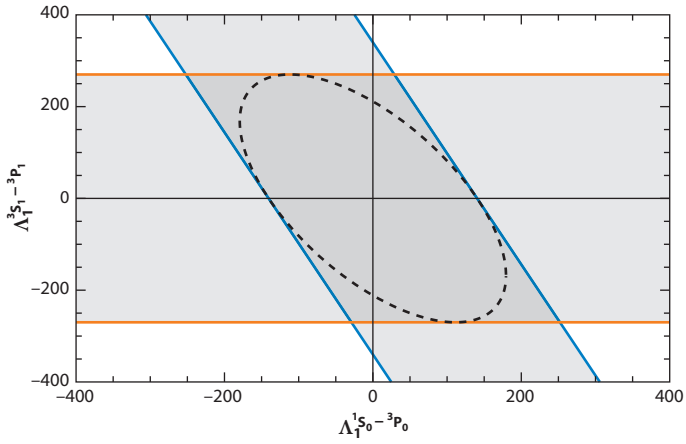

Figure 5

The progress in constraining the large-N_c isovector next-to-next-to-leading order low-energy constants (LECs) that will result from a combination of anticipated NPDGamma results (*horizontal band*) with the existing constraint from $P_\gamma(^{18}\mathrm{F})$ (*oblique band*). The former assumes a central value of zero for $A_\gamma(\vec{n}p \to d\gamma)$ and an uncertainty determined by the experiment's statistics, and thus assumes that the current campaign to subtract out window-induced asymmetries will yield a final systematic uncertainty well below the statistical uncertainty. Note that both isovector LECs are bounded once the NPDGamma results are combined with $P_\gamma(^{18}\mathrm{F})$, whereas neither is bounded without the former result. The LECs are in units of 10^{-7}.

Figure 5 also shows that the NPDGamma result is essential in placing such bounds on $\Lambda_1^{^1S_0-{}^3P_0}$ and $\Lambda_1^{^3S_1-{}^3P_1}$: $P_\gamma(^{18}\mathrm{F})$ by itself constrains neither to be below the LO scale. The two measurements are highly complementary, testing distinct combinations of the $\Delta I = 1$ LECs.

Next-generation experiments aiming to reach the N^{2}LO level will be challenging, and would be more easily motivated if the needed sensitivity to see N^{2}LO contributions could be better defined. If current LQCD efforts to determine $\Lambda_2^{^1S_0-{}^3P_0}$ at the 10% level meet with success, then the N^{2}LO contributions might be the next LQCD challenge. Although the presence of disconnected diagrams would substantially increase the difficulty of $\Delta I = 1$ calculations, the detection of a signal of any quality would be helpful to the field, as they would potentially confirm the predicted large-N_c coupling hierarchy and provide a definite target for the experimentalists.

4.3. The Potential Impact of New Experiments

Several recent proposals have been made to initiate new experiments, and others have been pursued or discussed in the past. The large-N_c LEC hierarchy can be used to determine how new experiments will affect our understanding of hadronic PNC. We first describe some of the potential observables:

1. An effort to measure the longitudinal asymmetry for scattering polarized neutrons from a ^{3}He target—$\vec{n} + {}^3\mathrm{He} \to {}^3\mathrm{H} + p$—is under way at the SNS. The predicted value, based on calculations by Viviani et al. (97) using the AV18 potential with the UIX three-body interaction, is

$$\frac{364}{10^{-8}} A_p = -\Lambda_0^+ + 0.227\Lambda_2^{^1S_0-{}^3P_0} - \left[3.82\Lambda_0^- + 8.18\Lambda_1^{^1S_0-{}^3P_0} + 2.27\Lambda_1^{^3S_1-{}^3P_1}\right]. \qquad 25.$$

Using the best-fit parameters for the two LO LECs yields $A_p \sim -1.8 \times 10^{-8}$. As the relative sign of the two LO LECs is opposite to that found for $A_{\rm L}(\vec{p}p)$, a measurement would generate a complementary band in **Figure 3**, testing the region of intersection identified there.

2. There was a past attempt to detect the γ-ray asymmetry produced when longitudinally polarized neutrons capture on a deuterium target, $\vec{n} + d \rightarrow t + \gamma$. $A_\gamma(\vec{n}d)$ is a rare example of a few-nucleon PNC observable where some enhancement occurs, as the parity-conserving M1 amplitude is suppressed at thermal neutron energies. The predicted asymmetry is (98)

$$\frac{118}{10^{-7}} A_\gamma = \Lambda_0^+ + 0.44\Lambda_2^{^1\mathrm{S}_0-{}^3\mathrm{P}_0} - \left[1.86\Lambda_0^- + 0.65\Lambda_1^{^1\mathrm{S}_0-{}^3\mathrm{P}_0} + 0.42\Lambda_1^{^3\mathrm{S}_1-{}^3\mathrm{P}_1}\right], \qquad 26.$$

yielding $\sim 7.3 \times 10^{-7}$ for the LO best values. The value obtained in an experiment by Avenier et al. (56), $\sim 8 \times 10^{-6}$, is an order of magnitude larger. This result has been largely ignored because of concerns about unidentified systematics (17).

3. There are several *np* observables complementary to NPDGamma's $A_\gamma(\vec{n}p)$. Significant effort has been invested in studies of the circular polarization of the 2.2-MeV γ-ray produced in thermal neutron capture on the proton. The circular polarization (57),

$$\frac{825}{10^{-7}} P_\gamma = \Lambda_0^+ + 1.27\Lambda_2^{^1\mathrm{S}_0-{}^3\mathrm{P}_0} + \left[0.47\Lambda_0^-\right], \qquad 27.$$

is $\sim 1.4 \times 10^{-7}$ for the LO LEC best values. The combination of three separate measurements and various control experiments by Knyaz'kov et al. (55) led to a determination of $P_\gamma = (1.8 \pm 1.8) \times 10^{-7}$, superseding an earlier result that apparently was contaminated by bremsstrahlung from the reactor core (99). Recently, interest has been expressed in measuring the inverse reaction, the circular polarization dependence of the breakup reaction $\vec{\gamma}d \rightarrow n + p$, which of course has an identical dependence on the LECs. This has been proposed as a commissioning experiment at an upgraded HIγS facility (100).

4. The neutron spin rotation of polarized cold neutrons traversing a parahydrogen target is a third possible *np* observable. The experiment is feasible because strong interaction spin-flip scattering off parahydrogen ($S = 0$ molecules) is forbidden. The spin rotation, taken from the Paris potential results of Reference 101 as modified by References 102 and 103 (see also References 58, 104, and 105),

$$\frac{180}{10^{-7}} \frac{\mathrm{d}\phi^n}{\mathrm{d}z}\bigg|_{\rm parahydrogen} = \left(\Lambda_0^+ + 2.82\Lambda_2^{^1\mathrm{S}_0-{}^3\mathrm{P}_0} - \left[3.15\Lambda_0^- + 1.94\Lambda_1^{^3\mathrm{S}_1-{}^3\mathrm{P}_1}\right]\right) \mathrm{rad\,m^{-1}}, \qquad 28.$$

is $\sim 9.1 \times 10^{-7}$ rad m^{-1} for the best-value LO LECs. To date, no experiment has been mounted. This is also the case with a fourth possible *np* observable, the dependence of the capture cross section on the neutron helicity, which tests a combination of LECs identical to that appearing above. Note that the neutron spin rotation in deuterium has also been calculated (106).

5. A neutron spin rotation experiment has been attempted in ^{4}He (107), where

$$\frac{105}{10^{-7}} \frac{\mathrm{d}\phi^{\rm n}}{\mathrm{d}z}\bigg|_{^4\mathrm{He}} = \left(\Lambda_0^+ - \left[1.61\Lambda_0^- + 0.92\Lambda_1^{^1\mathrm{S}_0-{}^3\mathrm{P}_0} + 0.35\Lambda_1^{^3\mathrm{S}_1-{}^3\mathrm{P}_1}\right]\right) \mathrm{rad\,m^{-1}}, \qquad 29.$$

leading to a predicted LO spin rotation of 6.8×10^{-7} rad m^{-1}. The experiment, performed on the slow neutron beam line at NIST, established an upper bound of $(1.7 \pm 9.1 \pm 1.4) \times 10^{-7}$ rad m^{-1} (54).

Table 3 Candidate future hadronic parity nonconservation experiments, including several that have been or are now being pursued[a]

Observable	Experimental status	LO expectation	LO LEC dependence
$A_p(\vec{n}+{}^3\mathrm{He}\to{}^3\mathrm{H}+p)$	Ongoing	-1.8×10^{-8}	$-\Lambda_0^+ + 0.227\Lambda_2^{^1S_0-{}^3P_0}$
$A_\gamma(\vec{n}+d\to t+\gamma)$	8×10^{-6} (56)	7.3×10^{-7}	$\Lambda_0^+ + 0.44\Lambda_2^{^1S_0-{}^3P_0}$
$P_\gamma(n+p\to d+\gamma)$	$(1.8\pm1.8)\times10^{-7}$ (55)	1.4×10^{-7}	$\Lambda_0^+ + 1.27\Lambda_2^{^1S_0-{}^3P_0}$
$\left.\frac{d\phi^n}{dz}\right\|_{\text{parahydrogen}}$	None	9.4×10^{-7} rad m^{-1}	$\Lambda_0^+ + 2.7\Lambda_2^{^1S_0-{}^3P_0}$
$\left.\frac{d\phi^n}{dz}\right\|_{^4\mathrm{He}}$	$(1.7\pm9.1\pm1.4)\times10^{-7}$ (54)	6.8×10^{-7} rad m^{-1}	Λ_0^+
$A_L(\vec{p}+d)$	$(-3.5\pm8.5)\times10^{-8}$ (41)	-4.6×10^{-8}	$-\Lambda_0^+$

[a]The leading-order (LO) large-N_c estimates for the observables are given, along with the functional dependence on the low-energy constants (LECs).

6. The longitudinal analyzing power for the scattering of polarized protons on deuterium, where (108)

$$\frac{156}{10^{-8}}A_L = -\Lambda_0^+ + \left[1.75\Lambda_0^- - 1.09\Lambda_1^{^1S_0-{}^3P_0} - 1.25\Lambda_1^{^3S_1-{}^3P_1}\right], \qquad 30.$$

leads to an LO large-N_c estimate of $A_L = -4.6\times10^{-8}$. An experiment was performed at 15 MeV nearly 40 years ago, yielding the result $A_L = (-3.5\pm8.5)\times10^{-8}$ (41).

A summary of this discussion is presented in **Table 3**. All of the above experiments belong in the same class as those displayed in **Figure 3**, presumably dominated by the LO LECs. Thus, it would be appropriate to set goals, for future efforts on these observables, that will guarantee they improve the pattern in that figure. To be competitive, uncertainties should then be achieved that are at least comparable to those of the $A_L(\vec{p}\alpha)$ and $A_\gamma(^{19}\mathrm{F})$ measurements, which, as noted above, are ~25%. The last two experiments in the table are sensitive only to Λ_0^+, and thus can be viewed as surrogates for $A_L(\vec{p}\alpha)$ and $A_\gamma(^{19}\mathrm{F})$. As we have argued that it is important to reduce the errors on these measurements to ~10%, better defining the two LO LECs, one might consider whether that goal could be reached more easily via $A_L(\vec{p}d)$ or neutron spin rotation in ^{4}He.

Four of the experiments depend on linear combinations of Λ_0^+ and $\Lambda_2^{^1S_0-{}^3P_0}$, and in three cases these combinations are not too different from that tested in $A_L(\vec{p}p)$. Consequently, not much will be learned unless an ~10% uncertainty comparable to that of $A_L(\vec{p}p)$ is achieved. The observable $A_p(\vec{n}+{}^3\mathrm{He}\to{}^3\mathrm{H}+p)$, which is the subject of an ongoing experiment (see **http://online.kitp.ucsb.edu/online/nuclear-c16/**), is notable because the contributions from Λ_0^+ and $\Lambda_2^{^1S_0-{}^3P_0}$ carry opposite signs. A high-quality result would place a fifth band on **Figure 3**, oblique to those now there. That would be very helpful in testing the large-N_c picture. An uncertainty on $A_p(\vec{n}+{}^3\mathrm{He}\to{}^3\mathrm{H}+p)$ of $\lesssim1\times10^{-8}$ would have a major impact on **Figure 3**.

All of these remarks are made under the assumption that N^{2}LO corrections are indeed of the naïvely expected size, ~10%. If this assumption is wrong, then the question of the role of candidate new experiments becomes more complicated. We also remark that none of the experiments in **Table 3** is like ^{18}F and NPDGamma, which are exclusively sensitive to N^{2}LO corrections. This underscores the importance of these two experiments, providing a unique opportunity to establish the scales of two of the three N^{2}LO LECs cleanly and, thus, to verify the predicted large-N_c LEC hierarchy.

5. SUMMARY AND OUTLOOK

The field of hadronic PNC began threescore years ago, when it was recognized that the weak semileptonic interaction responsible for nuclear β decay violates parity and that there should exist a corresponding parity-violating signal in the *NN* interaction due to the nonleptonic weak force. By exploiting parity violation, it was realized that one could isolate this interaction despite its embedding in a strongly interacting system, testing our understanding of *W* and *Z* boson exchange among the quarks. *NN* and nuclear systems were recognized as uniquely important to the study of the neutral current, which plays no role in strangeness-changing interactions due to the absence of flavor-changing neutral currents. For many years it has been anticipated that the neutral current would be revealed in a PNC $\Delta I = 1$ interaction of long range, generated by pion exchange. The expectation that this interaction would have important consequences for PNC observables has influenced PNC analyses since the 1980s. Yet, the combination of experimental data, large-N_c arguments, and subsequent reexaminations of QCD effects influencing the size of h_π^1 indicates otherwise.

Experimental progress in this field has been slow due to the difficulty of measuring effects with a natural size of order $(Gm_\pi^2) \sim 10^{-7}$ relative to the strong interaction: Despite the distinctive character of PNC observables, there are many systematics that can lead to false signals at this level. On the theoretical side, one had the challenge of five independent S–P Danilov amplitudes, and very few measurements to constrain these amplitudes. There was a need to find some organizing principle to simplify this task. Influenced by meson-exchange models of PNC, the interest in the $\Delta I = 1$ interaction, and the absence of $\Delta I = 2$ contributions to the data displayed in **Figure 3** [apart from $A_L(\vec{p}p)$], the choice was made to focus on average $\Delta I = 0$ and 1 strengths, reducing the S–P interaction to two effective couplings. Compounded by some inconsistent treatments of couplings, resolved only recently (3), this led to a puzzling pattern, including the conclusion that the $\Delta I = 1$ degree of freedom was unneeded.

Meson-exchange models such as the DDH potential attempt to predict weak couplings, a daunting task given the uncertainties inherent in embedding weak interactions in a strongly interacting environment. Beginning about 10 years ago, pionless EFTs began to be employed. As noted in this review, this approach is closely related to the Danilov amplitudes and to the contact potential of Desplanques & Missimer (37), which date to the field's early days. Furthermore, the DDH potential is operationally identical to pionless EFT, in the S–P limit. Thus, one could argue that there is little new in the EFT approach. By contrast, EFT forces one to again confront the issue of five independent *S–P* amplitudes: There is no organizational principle in EFT for reducing the number of LECs to a more manageable number. The LECs appear as equivalent constants that must be determined from experiment.

This is why the recent application of large N_c to the PNC is such an important step forward: It provides a hierarchical division of the LECs into two groups, two LO LECs with $\Delta I = 0$ and $\Delta I = 2$, and three N^{2}LO LECs that naïvely are ~10% corrections, two of which carry $\Delta I = 1$ and one $\Delta I = 0$. The purpose of this review has been to apply this formalism to the full body of information available on PNC. The LO LECs—Λ_0^+ and $\Lambda_2^{^1S_0-{}^3P_0}$—can be reasonably well determined from existing PNC results, and the resulting LO large-N_c effective theory accounts for all of the existing measurements. We have also argued that the remaining three constants—$\Lambda_1^{^1S_0-{}^3P_0}$, $\Lambda_1^{^3S_1-{}^3P_1}$, and Λ_0^-—do indeed contribute at a suppressed level. More precisely, if NPDGamma produces a result close to its announced statistical precision, it can be combined with $P_\gamma(^{18}\mathrm{F})$ to constrain $\Lambda_1^{^1S_0-{}^3P_0}$ and $\Lambda_1^{^3S_1-{}^3P_1}$ to values considerably below that of Λ_0^+.

In retrospect, the field has been very fortunate in its choice of experiments. $A_{\rm L}(\vec{p}\,p)$, $A_{\rm L}(\vec{p}\alpha)$, and $A_\gamma(^{19}{\rm F})$ have allowed us to extract the large-N_c LO LECs. $P_\gamma(^{18}{\rm F})$ and $A_\gamma(\vec{n}\,p \to d\gamma)$ probe the N^{2}LO $\Delta I = 1$ plane in complementary ways, potentially allowing us to demonstrate the LEC hierarchy suggested by large N_c by constraining two of the subdominant LECs.

It strikes us that, after many years during which the theoretical and experimental situations were less clear, we are beginning to understand the pattern of PNC in *NN* systems. There are opportunities to make further progress—to pick experiments that optimally constrain the LECs and test the patterns predicted by large N_c. These include the following:

1. An LQCD evaluation of the couplings, beginning with a measurement of the $\Delta I = 2$ parameter $\Lambda_2^{^1{\rm S}_0-{}^3{\rm P}_0}$. A measurement accurate to 10% would significantly narrow the uncertainties on Λ_0^+ and $\Lambda_2^{^1{\rm S}_0-{}^3{\rm P}_0}$. This calculation is the natural first step for LQCD, as the $\Delta I = 2$ amplitude has no contributions from disconnected (quark -loop) diagrams.
2. An improved determination of the LO parameters Λ_0^+ and $\Lambda_2^{^1{\rm S}_0-{}^3{\rm P}_0}$ by a modern and higher-precision measurement of the $\vec{p}\alpha$ longitudinal analyzing power and/or the ^{19}F photon decay asymmetry.
3. Alternatively, an improved determination of the LO parameters Λ_0^+ and $\Lambda_2^{^1{\rm S}_0-{}^3{\rm P}_0}$ by one of the new experiments listed in **Table 3**. We have noted that $A_{\rm L}(\vec{n} + {}^3{\rm He} \to {}^3{\rm H} + p)$, an experiment that is running now at the SNS, is a particularly good choice.
4. A test of the N^{2}LO parameters $\Lambda_1^{^1{\rm S}_0-{}^3{\rm P}_0}$, $\Lambda_1^{^3{\rm S}_1-{}^3{\rm P}_1}$, and Λ_0^- by a modern and higher-precision ^{18}F circular polarization measurement and/or a second-generation $\vec{n}\,p \to d\gamma$ experiment that limits statistical and systematic errors to $\lesssim 0.5 \times 10^{-8}$.

Undertaking all or some combination of these efforts could confirm the large-N_c picture outlined herein and provide accurate values for four of its five LECs. This in turn could finally demonstrate that the six-decade-long program to understand hadronic PNC has been successful.

DISCLOSURE STATEMENT

The authors are not aware of any affiliations, memberships, funding, or financial holdings that may be perceived as affecting the objectivity of this review.

ACKNOWLEDGMENTS

The authors acknowledge the hospitality of the Kavli Institute for Theoretical Physics and support from the National Science Foundation under award PHY11-25915. The work of S.G. was supported by the US Department of Energy under award DE-FG02-96ER40989. The work of W.C.H. was supported by the US Department of Energy under awards DE-SC00046548, DE-AC02-98CH10886, and KB0301052 and by grant 394310 from the Simons Foundation. The authors thank Chris Crawford for his careful reading of the manuscript.

LITERATURE CITED

1. Fry J, et al. *Hyperfine Interact.* 238(1):11 (2017)
2. Kurth T, et al. *Proc. Sci.* LATTICE2015:329 (2016)
3. Haxton W, Holstein B. *Prog. Part. Nucl. Phys.* 71:185 (2013)
4. Phillips DR, Samart D, Schat C. *Phys. Rev. Lett.* 114:062301 (2015)
5. Schindler MR, Springer RP, Vanasse J. *Phys. Rev. C* 93:025502 (2016)

6. Donoghue JF, Golowich E, Holstein BR. *Camb. Monogr. Part. Phys. Nucl. Phys. Cosmol.* 2:1 (1992)
7. Maiani L. *Riv. Nuovo Cim.* 34:679 (2011)
8. Desplanques B, Donoghue JF, Holstein BR. *Ann. Phys.* 124:449 (1980)
9. Barnes C, et al. *Phys. Rev. Lett.* 40:840 (1978)
10. Bizetti PG, et al. *Lett. Nuovo Cim.* 29:167 (1980)
11. Ahrens G, et al. *Nucl. Phys. A* 390:486–508 (1982)
12. Bini M, Fazzini T, Poggi G, Taccetti N. *Phys. Rev. Lett.* 55:795 (1985)
13. Page S, et al. *Phys. Rev. C* 35:1119 (1987)
14. Haxton W. *Phys. Rev. Lett.* 46:698 (1981)
15. Bennett C, Lowrey MM, Krien K. *Bull. Am. Phys. Soc.* 25:486 (1980)
16. Adelberger E, et al. *Phys. Rev. C* 27:2833–56 (1983)
17. Adelberger EG, Haxton WC. *Annu. Rev. Nucl. Part. Sci.* 35:501 (1985)
18. Gericke M, et al. *Phys. Rev. C* 83:015505 (2011)
19. Page SA, et al. *J. Res. Natl. Inst. Stand. Technol.* 110:195 (2005)
20. Caviagnac JF, Vignon B, Wilson R. *Phys. Lett. B* 67:149 (1977)
21. Zhu S-L, et al. *Nucl. Phys. A* 748:435 (2005)
22. Girlanda L. *Phys. Rev. C* 77:067001 (2008)
23. Phillips DR, Schindler MR, Springer RP. *Nucl. Phys. A* 822:1 (2009)
24. Danilov G. *Phys. Lett.* 18:40 (1965)
25. Danilov G. *Phys. Lett. B* 35:579 (1971)
26. Danilov G. *Sov. J. Nucl. Phys.* 14:443 (1972)
27. Lee TD, Yang C-N. *Phys. Rev.* 104:254 (1956)
28. Wu CS, et al. *Phys. Rev.* 105:1413 (1957)
29. Tanner N. *Phys. Rev.* 107:1203 (1957)
30. Haeberli W, Holstein BR. arXiv:nucl-th/9510062 (1995)
31. Ramsey-Musolf MJ, Page SA. *Annu. Rev. Nucl. Part. Sci.* 56:1 (2006)
32. Krane K, Olsen C, Sites JR, Steyert W. *Phys. Rev. Lett.* 26:1579 (1971)
33. Yuan V, et al. *Phys. Rev. C* 44:2187 (1991)
34. Dubovik VM, Zenkin SV. *Ann. Phys.* 172:100 (1986)
35. Feldman GB, Crawford GA, Dubach J, Holstein BR. *Phys. Rev. C* 43:863 (1991)
36. Schindler M, Springer R. *Prog. Part. Nucl. Phys.* 72:1 (2013)
37. Desplanques B, Missimer JH. *Nucl. Phys. A* 300:286 (1978)
38. Wasem J. *Phys. Rev. C* 85:022501 (2012)
39. Carlson J, Schiavilla R, Brown V, Gibson B. *Phys. Rev. C* 65:035502 (2002)
40. Eversheim P, et al. *Phys. Lett. B* 256:11 (1991)
41. Nagle D, et al. *AIP Conf. Proc.* 51:224 (1979)
42. Balzer R, et al. *Phys. Rev. Lett.* 44:699 (1980)
43. Balzer R, et al. *Phys. Rev. C* 30:1409 (1984)
44. Kistryn S, et al. *Phys. Rev. Lett.* 58:1616 (1987)
45. Berdoz AR, et al. *Phys. Rev. C* 68:034004 (2003)
46. Berdoz AR, et al. *Phys. Rev. Lett.* 87:272301 (2001)
47. Lang J, et al. *Phys. Rev. Lett.* 54:170 (1985)
48. Henneck R, et al. *Phys. Rev. Lett.* 48:725 (1982)
49. Elsener K, et al. *Nucl. Phys. A* 461:579 (1987)
50. Elsener K, et al. *Phys. Rev. Lett.* 52:1476 (1984)
51. Wood C, et al. *Science* 275:1759 (1997)
52. Snover KA, et al. *Phys. Rev. Lett.* 41:145 (1978)
53. Earle ED, et al. *Nucl. Phys. A* 396:221C (1983)
54. Snow W, et al. *Phys. Rev. C* 83:022501 (2011)
55. Knyaz'kov VA, et al. *Nucl. Phys. A* 417:209 (1984)
56. Avenier M, et al. *Phys. Lett. B* 137:125 (1984)

57. Desplanques B. *Nucl. Phys. A* 335:147 (1980)
58. Liu CP. *Phys. Rev. C* 75:065501 (2007)
59. de Vries J, et al. *Phys. Lett. B* 747:299 (2015)
60. McKellar B. *Phys. Lett. B* 26:107 (1967)
61. Fischbach E. *Phys. Rev.* 170:1398 (1968)
62. Tadić D. *Phys. Rev.* 174:1694 (1968)
63. Kummer W, Schweda M. *Acta Phys. Aust.* 28:303 (1968)
64. Fischbach E, Tadić D. *Phys. Rep.* 6:123 (1973)
65. Box MA, McKellar BHJ, Pick P, Lassey KR. *J. Phys. G* 1:493 (1975)
66. Patrignani C, et al. (Part. Data Group) *Chin. Phys. C* 40:100001 (2016)
67. Donoghue JF, Golowich E, Holstein B. *Phys. Rep.* 131:319 (1986)
68. Barton G. *Nuovo Cim.* 19:512 (1961)
69. Glashow SL, Iliopoulos J, Maiani L. *Phys. Rev. D* 2:1285 (1970)
70. Kaplan DB, Savage MJ. *Nucl. Phys. A* 556:653 (1993)
71. Kaiser N, Meißner U-G. *Nucl. Phys. A* 489:671 (1988)
72. Meißner UG, Weigel H. *Phys. Lett. B* 447:1 (1999)
73. Freeman W, Toussaint D. (MILC Collab.) *Phys. Rev. D* 88:054503 (2013)
74. Ohki H, et al. (JLQCD Collab.) *Phys. Rev. D* 87:034509 (2013)
75. Junnarkar P, Walker-Loud A. *Phys. Rev. D* 87:114510 (2013)
76. Gong M, et al. (XQCD Collab.) *Phys. Rev. D* 88:014503 (2013)
77. Dai J, Savage MJ, Liu J, Springer RP. *Phys. Lett. B* 271:403 (1991)
78. Buchalla G, Buras AJ, Lautenbacher ME. *Rev. Mod. Phys.* 68:1125 (1996)
79. Boyle PA, et al. *Phys. Rev. Lett.* 110:152001 (2013)
80. Buras AJ, Gerard J-M, Bardeen WA. *Eur. Phys. J. C* 74:2871 (2014)
81. Maiani L, Testa M. *Phys. Lett. B* 245:585 (1990)
82. Huang K, Yang CN. *Phys. Rev.* 105:767 (1957)
83. Lee TD, Huang K, Yang CN. *Phys. Rev.* 106:1135 (1957)
84. Wu TT. *Phys. Rev.* 115:1390 (1959)
85. Lüscher M. *Commun. Math. Phys.* 105:153 (1986)
86. Lüscher M. *Nucl. Phys. B* 354:531 (1991)
87. Berkowitz E, et al. *Phys. Lett. B* 765:285 (2017)
88. Tiburzi B. *Phys. Rev. D* 86:097501 (2012)
89. Kaplan DB, Savage MJ, Wise MB. *Phys. Lett. B* 424:390 (1998)
90. Epelbaum E, Gloeckle W, Meißner U-G. *Nucl. Phys. A* 637:107 (1998)
91. Epelbaum E, Gloeckle W, Meißner U-G. *Nucl. Phys. A* 671:295 (2000)
92. van Kolck U. *Prog. Part. Nucl. Phys.* 43:337 (1999)
93. Beane SR, Bedaque PF, Savage MJ, van Kolck U. *Nucl. Phys. A* 700:377 (2002)
94. Epelbaum E, Hammer H-W, Meißner U-G. *Rev. Mod. Phys.* 81:1773 (2009)
95. Beane SR, Savage MJ. *Nucl. Phys. B* 636:291 (2002)
96. Marcucci LE, Nollett KM, Schiavilla R, Wiringa RB. *Nucl. Phys. A* 777:111 (2006)
97. Viviani M, et al. *Phys. Rev. C* 82:044001 (2010)
98. Desplanques B, Benayoun JJ. *Nucl. Phys. A* 458:689 (1986)
99. Lobashov VM, et al. *Nucl. Phys. A* 197:241 (1972)
100. Snow WM, et al. *Int. J. Mod. Phys. Conf. Ser.* 40:1660002 (2016); Vanasse J, Schindler MR. *Phys. Rev. C* 90:044001 (2014)
101. Avishai Y, Grange P. *J. Phys. G* 10:L263 (1984)
102. Heckel B. In *Proceedings of the Workshop on the Investigation of Fundamental Interactions with Cold Neutrons*, ed. GL Greene, p. 90. Washington, DC: Natl. Bur. Stand. (1986)
103. Adelberger E. In *Proceedings of the Symposium/Workshop on Parity Violation in Hadronic Systems*, ed. SA Page, WD Ramsay, WTH Van Oers, p. 50. Vancouver, Can.: TRIUMF (1987)
104. Schiavilla R, Carlson J, Paris MW. *Phys. Rev. C* 70:044007 (2004)

105. Griesshammer HW, Schindler MR, Springer RP. *Eur. Phys. J. A* 48:7 (2012)
106. Schiavilla R, et al. *Phys. Rev. C* 78:014002 (2008); Schiavilla R, et al. Erratum. *Phys. Rev. C* 83:029902 (2011); Vanasse J. *Phys. Rev. C* 86:014001 (2012); Vanasse J. *Phys. Rev. C* 88:044001 (2013)
107. Dmitriev VF, Flambaum VV, Sushkov OP, Telitsin VB. *Phys. Lett. B* 125:1 (1983)
108. Desplanques B, Benayoun JJ, Gignoux C. *Nucl. Phys. A* 324:221 (1979)